Stony Brook University

Evaluation of Contrast Agents Used in Computed Tomography

A Dissertation Presented

by

Michael J. Bonvento

to

The Graduate School

in Partial Fulfillment of the

Requirements

for the Degree of

Doctor of Philosophy

in

Biomedical Engineering

Stony Brook University

May 2016

Stony Brook University
The Graduate School

Michael J. Bonvento

We, the dissertation committee for the above candidate for the
Doctor of Philosophy degree, hereby recommend
acceptance of this dissertation.

_____
Terry M. Button, Ph.D. – Dissertation Advisor
Associate Professor, Biomedical Engineering Department

_____
Wei Zhao, Ph.D. - Chairperson of Defense
Professor, Biomedical Engineering Department

_____
F. Avraham Dilmanian, Ph.D.
Professor, Biomedical Engineering Department

_____
Sachin Jambawalikar, Ph.D.
Assistant Professor of Radiology, Columbia University Medical Center

This dissertation is accepted by the Graduate School

_____
Charles Taber
Dean of the Graduate School

Abstract of the Dissertation

Evaluation of Contrast Agents Used in Computed Tomography

by

Michael J. Bonvento

Doctor of Philosophy

in

Biomedical Engineering

Stony Brook University

2016

Contrast agents have been routinely employed in radiographic applications for more than 80 years and in computed tomography (CT) for more than 50 years. These agents have high atomic number increasing the photoelectric interaction probability thereby reducing photon intensity projected through the contrast containing structure and improving available image contrast. A wide variety of contrast agents have been examined over the years, however, iodine and barium containing agents make up the vast majority of applications. Other agents are or may become available which may find utility due to reduced toxicity, better characteristics for imaging or dose reduction. This is particularly true as computed tomography based angiography (CTA) replaces conventional angiography for diagnostic applications.

The purpose of this dissertation is to develop a frame work for the evaluation of new and future contrast agents as they apply to CT enhancement including CTA. The contrast agent evaluation model developed in this dissertation allows for the examination of potential new contrast agents as well as the optimized use of existing contrast agents. Optimization is

accomplished by examining the impact of kilovoltage and filter combinations on image quality and radiation dose. In this way the minimum concentration of contrast agent, at a given radiation dose, can be determined.

The approach taken was to model the spectra from an x-ray tube at a specified kilovoltage, compute the spectra after filtration and project the computed spectra through a cylindrically symmetric head phantom (16 cm diameter solid water) with a contrast containing target at its center. Noise was applied to projection data based on photon counting. Standard filtered back projection applied to the projection data provides a simulated image from which image contrast-to-noise ratio (CNR_i) can be determined. Alternatively, the projection data contrast-to-noise ratio (CNR_p) can be scaled with an empirically derived factor that accounts for propagation of error and other sources of error in the image formation process to obtain the CNR_i. Radiation dose at the center of the phantom was computed from photon fluence attenuated by 8 cm of water and empirically corrected for scatter radiation. An arbitrary target CNR_i of unity was selected and allowed for calculation of the target contrast agent concentration that resulted in a CNR of unity per unit radiation dose. We have defined the resulting contrast agent concentration as the minimum effective concentration (MEC). With this model the impact of x-ray beam kilovoltage and filtration on MEC can be determined by computation, thereby allowing for their optimization.

The model has been validated with a phantom using direct measurement of dose and contrast using a clinical CT system. From the contrast agent evaluation model, an improved understanding of the potential to optimize iodine contrast enhancement was gained. Likewise, the potential use of gadolinium as a CT contrast agent has been recognized. Finally the contrast agent enhancement model has been used to predict how gadolinium enhanced CT can be greatly improved through the use of the appropriate kilovoltage and filter combination.

Table of Contents

Figures

Tables

Abbreviations

mR	milliroentgen(s)	A unit of radiation exposure
CT	Computerized Tomography	
keV	kiloelectron volts	A unit of energy
kVp	kilovolts peak	Potential energy applied to the x-ray tube
MRI	Magnetic Resonance Imaging	
NSF	nephrogenic systemic fibrosis	
MDCT	Multi-Detector Computerized Tomography	
CTA	Computerized Tomography Angiography	
CNR	Contrast-to-Noise Ratio	
TLD	Thermoluminescent Dosimeter	
MEC	Minimum Effective Concentration	
cGy	centigray	A unit of radiation dose
HVL	Half-Value Layer	Measured in millimeters of aluminum
ROI	Region of Interest	
mAs	milliamper-second(s)	product of tube current and exposure time
mM	millimol	
CNR_i	Contrast-to-Noise Ratio in the Image	
CNR_p	Contrast-to-Noise Ratio in the Projection Data	

Acknowledgments

I am indebted to the many people with whom I have worked on the papers and presentations that have culminated in the preparation of this proposal: Terry M. Button, Ph.D., Avraham Dilmanian, Ph.D., William H. Moore, M.D., Renat Yakupov, and Rosemarie Oliviere-Fitt, M.D. I am also indebted to Sachin Jambawalikar Ph.D. for his invaluable assistance in generating simulated CT images. Finally, I want to acknowledge and thank my Dissertation Committee: Wei Zhao, Ph.D., Chair; Terry M. Button, Ph.D., Advisor; Avraham Dilmanian, Ph.D.; Sachin Jambawaliker, Ph.D.; and Edward L. Nickoloff, D.Sc. for their support and assistance.

1. Introduction

1.1 Contrast Agents in CT

1.1.1 X-ray Tube Physics

X-radiation is produced by bombarding a target with high energy electrons[1]. There are two mechanisms for this production: bremstrahlung and characteristic x-ray production. Bremstrahlung radiation is the result of the deceleration of the charged particle as it approaches the electrostatic field of the target nucleus. Since the deceleration of electrons depends on their distance from the target nucleus and initial velocity, the resulting x-ray energy will range from a value approaching zero to a maximum that is the energy of the incident electron. The maximum energy occurs when the electron is completely stopped in the field of the nucleus. Alternatively, characteristic x-rays can be produced when electrons have sufficient energy to ionize inner shell orbiting electrons. When the resulting vacancy is filled by an electron in one of the outer shells, the difference in binding energy between the shells may be released as a characteristic x-ray. An alternative to characteristic x-rays is the release of Auger electrons.

X-ray tubes require a source of electrons and a high potential difference to accelerate those electrons. This latter requirement is provided by a high voltage generator which includes a high current step down transformer and a high voltage step up transformer. The key components of an x-ray tube used for medical imaging include:

1. Source of Electrons

Electrons are used in medical imaging x-ray tubes as the accelerated charged particles. A coiled filament of tungsten wire is heated using a low voltage and high current from the high current step down transformer to a produce a high temperature for thermionic emission of electrons. The filament is placed inside a focusing cup. This cup is the negative terminal of the high voltage generator. Prior to the initiation of a radiation exposure, thermionic emission results in a cloud of electrons surrounding the filament. When a high potential difference generated by the high voltage transformer is placed between the cathode assembly (filament and focusing cup) and the target, the electrons are accelerated to the target. The maximum potential difference determines the maximum energy of the electrons and, therefore, the maximum energy of the resulting x-radiation[2]. The focusing cup brings the electrons to bear on a small region of the target called the focal spot.

2. Target

The target (anode) of the x-ray tube is characterized by two important physical features. First, it has a high atomic number. This is important because the efficiency of x-ray production is roughly proportional to Z. Second, the material must have a very high melting point because; at the energies used for medical imaging more than 99% of the energy that is produced is heat. Tungsten (and combinations of tungsten with rhenium) is often employed for imaging applications[3] although mammographic applications frequently use molybdenum[3]. Tungsten has a high atomic number (74) and, of all metals in pure form, tungsten has the highest melting point (3,422 °C, 6,192 °F), lowest vapor pressure and (at temperatures above 1,650 °C, 3,002 °F) the highest tensile strength.[4] Tungsten has the lowest coefficient of thermal expansion of any pure metal[5]. These are all advantageous in the high temperature environment of the x-ray tube target.

The tungsten target is generally mounted on a large, thick, circular disk of supporting material. The tungsten surface that is bombarded by the electrons is angled so as to produce a large surface area while maintaining a small effective focal spot size to assure high spatial resolution. During operation the disk will rotate at several thousand revolutions per minute. Rotating the anode allows the bombardment to occur over a large surface area, thereby minimizing the potential for melting the tungsten target[6].

A high potential difference is placed between the anode and cathode during operation. In computerized tomography applications this potential difference typically ranges between 80 and 140 kilovolts. The electrons are accelerated to the anode and x-rays are produced in the tungsten layer. The focal spot is the physical dimension of the electron beam as it strikes the target. The effective focal spot is smaller because the target is on an angle. This allows a large surface area to be used while minimizing the penumbra blur associated with a focal spot that is not a true point source of radiation[6].

3. Evacuated Envelope

The anode and cathode are enclosed in an evacuated housing constructed of either glass or metal[7]. A high vacuum is critical to the proper operation of the tube because any gas molecules in the tube will interact with the electrons, thereby decreasing their energy and decreasing the efficiency of x-ray production[7]. A small amount of gas in the tube can also cause an excess of tube heating which can lead to tube failure[7].

4. Radiolucent Window for the X-Rays to Pass Through

X-rays are produced in all directions, but only those from the target toward the patient are needed. To support this, those x-rays directed toward the patient pass through a glass and a port of low Z metal (e.g., beryllium). The port is designed to absorb as little radiation as possible

while maintaining the vacuum of the tube[7]. A thin, radiolucent, window keeps the insulating oil in the housing while allowing the x-rays to pass through[7].

5. Insulating Oil for the Conduction of Heat from the Tube

X-ray production is a relatively inefficient process at diagnostic radiology energies. The ratio of radiative (x-ray) production to collisional losses (heat) is approximately E*Z/820000 where Z is the target atomic number and E is the electron energy in keV[8]. At 120 keV with a tungsten target this results in 1% of the input energy being converted to x-rays. The remaining energy results in target heating[8] and this thermal energy escapes by radiation from the target. For a typical CT exposure 120 kV at 500 mA may be used. Since the power is voltage x current, 60kW is employed with 99% of that energy manifesting as heat! In order for the x-ray tube to be able to produce numerous exposures or to operate continuously for an extended period of time heat from the target radiates energy into the insulating oil which surrounds the tube. This hot oil dissipates this heat, through convection, to the housing where it is lost to the housing and then to the environs. High heat capacity tubes employ additional cooling systems such as heat exchangers which circulate the oil through coolant filled radiators. The coolant is then circulated to either an outside chiller or is exposed to the environs for further cooling[9].

6. Lead-lined Housing

X-ray production is essentially uniform in all directions from the target – but absorbed by the target in the forward directions. The anode angle does favor a forward direction but that does not eliminate x-rays from other directions. It is therefore necessary to enclose the tube in a lead-lined housing[7]. For x-ray tubes designated as "diagnostic type" the housing must provide, as a minimum protection, less than 100 mR in any one hour at 1 meter in any direction (with the port blocked) when the tube is operated at its maximum potential and maximum continuous tube

current. Computerized Tomography tubes are Diagnostic Type and must meet this specification[10].

7. Filtration

The x-ray beam, as it emerges from the target, is composed of a continuous spectrum of energies. The highest intensity is at the lowest energy whereas the maximum energy has the lowest intensity[2]. Low energy photons are not desirable for imaging purposes as they are completely absorbed by the patient and do not produce any image information. Exposure of the patient to these pointless radiations is unethical. It is therefore necessary to remove them from the beam before they reach the patient. The lowest energies are removed by the window, glass and tube port (inherent filtration). Filtration is added after the window to remove additional low-energy photons. Federal regulations require at least 2.5 mm of aluminum (or its equivalent) for tubes that operate above 70 kilovolts peak[10]. Computerized Tomographic units use proprietary combinations of aluminum, copper, and/or other materials in an effort to produce beams with high effective energy.

8. Collimator

Radiation needs to be confined to the anatomical area of interest in order to maximize image quality by minimizing scattered radiation from areas that are not being imaged and to minimize the radiation exposure received by the patient[11]. Computerized Tomography (CT) produces images of axial slices of anatomy; the thickness of these slices is controlled by the operator. Thin slices minimize scatter and improve resolution in the elevation plane of the image. In CT, collimation is achieved both at the x-ray tube and at the detector. The collimator septa at the detector serve to reduce the detection of scattered radiation.

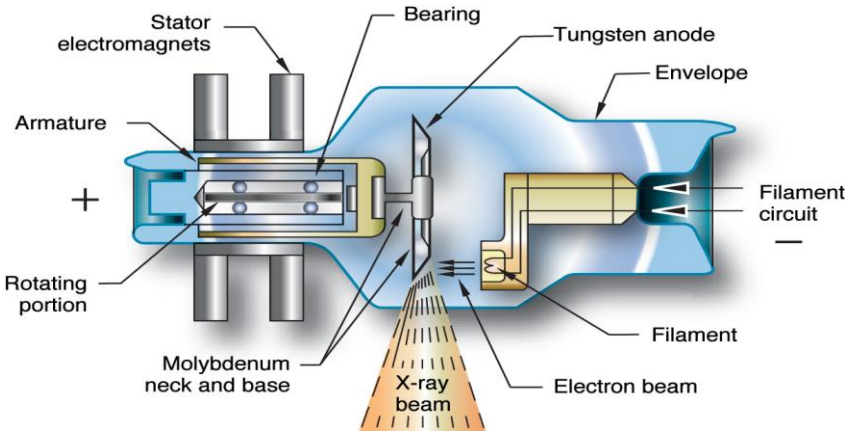

Diagram of an X-Ray Tube and its components

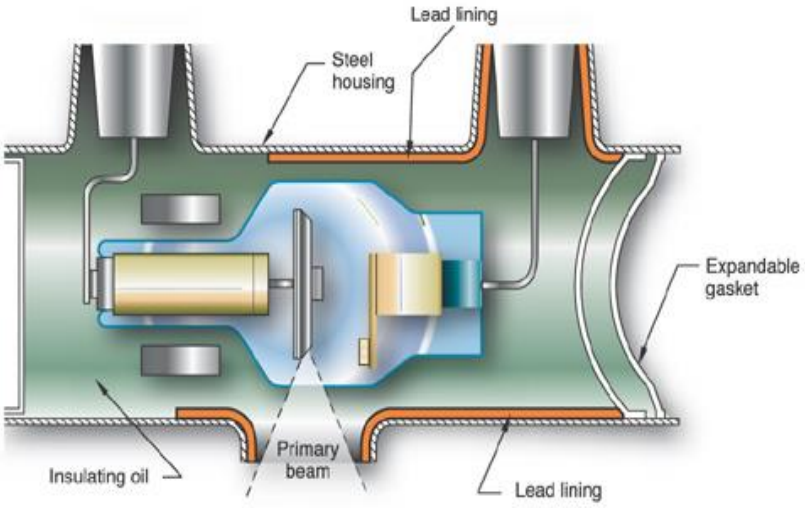

Figure 1 – Diagram of a medical x-ray tube and a tube within a tube housing (Figure 1 from CARLTON/ADLER. *Principles of Radiographic Imaging*, 4E. © 2006 Delmar Learning, a part of Cengage Learning, Inc. Reproduced by permission. www.cengage.com/permissions[12])

1.1.2 Contrast Agents

Very shortly after the discovery of x-rays by Roentgen in 1895 the utility of injectable contrast media was explored[13]. Perhaps the first report of radiography being performed with contrast media was in 1896. Haschеck and Lindenthal injected a mixture of mercury salts into

the vessels of an amputated hand[14]. The resulting radiograph clearly demonstrated the vascular structure. Subsequent work was performed throughout the early 20th century, with reports of femoral and cerebral angiography being performed in the 1920's with solutions of sodium bromide and strontium bromide as contrast media. Monitz reported the first cerebral angiography in 1927[14]. He used 7 ml of 70% strontium bromide for his first attempt. This compound did not opacify the vessels. Subsequently he used 5 ml of 25% sodium iodide and this compound achieved opacification. Monitz chose iodine as a contrast agent because of its high atomic number and concurrent radiation absorption properties. Sodium iodide, although useful as a contrast agent, required the patient to be under general anesthesia because it caused pain[, 15]. This disadvantage of sodium iodide led to the development and use of thorium dioxide as this compound is much better tolerated than salts of iodine. Thorium, however, is an alpha-emitting radioactive material and has a long effective half-life. Its use was discontinued in the 1950's when radiation induced carcinogenesis from this agent were fully appreciated[15].

In 1931, while developing iodine labeled compounds for antibiotic purposes, Binz noted that pyridine based compounds were excreted by both the kidneys and liver[15]. These molecules were investigated by Swick and Von Lichtenberg for urographic work and this led to the development of Uroselctan. Uroselectan and other products subsequently became the agents of choice for urography, angiography, and cerebral angiography[15].

In the early 1950's the first tri-iodinated contrast agents were developed. Acetrizoic acid was well tolerated and, with three iodine atoms per molecule, provided a great improvement in opacification. Ionic salts of tri-iodobenzoic acid were developed around the same time[13]. By the 1970's non-ionic iodinated media were being developed and introduced. These compounds do not disassociate and therefore have a lower osmolality than ionic media with the same number of

iodine atoms per molecule. This makes them better tolerated than ionic compounds[15]. Iodinated compounds provide radiographic subject contrast because of the high photoelectric cross-section of iodine in the energy range commonly used in diagnostic radiography. The k-edge of iodine is approximately 33 keV[16] which corresponds very nicely to the peak photon flux of x-radiation produced at 70 kVp filtered with 2.5 mm of aluminum (a typical set of parameters for general radiography). The mean photon energy of this beam is approximately 34 keV[17]. Iodine preferentially absorbs, through photoelectric interactions, photons above 33 keV which means that there will be considerable absorption of this spectrum by iodine. Tissue, however, is relatively transparent at this energy. The mass attenuation coefficient for iodine at 40 keV is 22.7 cm^2/gm and for muscle it is 0.267 cm^2/gm[16]. The photoelectric cross-section of iodine exceeds the Compton cross-section up to approximately 200 keV[16], which is well beyond the diagnostic range.

The aforementioned characteristics of iodinated material make it a popular choice for contrast – enhanced radiography. The applications of these media have increased since the recent development of computed tomography angiography (CTA) as an important imaging modality[18-21]. There are, however, several physiologic reactions to iodinated contrast material which are of concern. These can be divided into two categories: chemotoxic and osmotic effects[17]. Chemotoxic effects are those that are related directly to the chemistry of the contrast media. These can result in hives, cardiac arrhythmias, renal failure, allergic reactions and anaphylactoid shock[22, 23]. Osmotic effects are related to the number of particles in solution. The use of contrast material with high osmolality can result in shrinkage of red blood cells, the movement of fluid from the surrounding viscera into the blood vessels, and vasodilation[17]. Some other reactions of concern are sensations of pain and heat, vasodilatation and vasospasm,

changes in blood pressure and pulse rate, and interactions with blood and blood cells[17]. With most of these, the reactions appear to be less severe with non-ionic media than with ionic media. Since some of these reactions can be severe there is incentive to develop contrast media with less toxicity than the currently available iodinated materials.

The development of Magnetic Resonance Imaging (MRI) during the early 1980's led to the need for appropriate MRI contrast agents. In the case of MRI contrast agents, primarily altering relaxation properties rather than altering x-ray attenuation properties provides contrast. Chelates of gadolinium, such as Gd-DTPA, Gd-EDTA, and Gd-DOTA, have been used successfully as MRI contrast agents[24]. The advantages include water solubility, ready availability, and low toxicity. The safety profile of these compounds is, in fact, impressive with reports of up to 0.3 mmole/kg being used with no adverse effects[24-25]. Recently, however, gadolinium contrast agents have been associated with nephrogenic systemic fibrosis (NSF) in patients with severely diminished renal function[26]. These findings might present a limit to their utility for patients with renal insufficiency and could, in fact, make them contraindicated in these cases. Recent developments may, however, ameliorate this. A new gadolinium-based contrast agent, gadobenate dimeglumine, was shown in one study[27] to lower the risk of NSF. There is a considerable amount of research being conducted regarding the relative safety of gadolinium-based and iodine-based contrast agents for patients with varying degrees of renal impairment[28].

Absorption of x-radiation is a function of both atomic number and electron density with photoelectric processes being more highly dependent on atomic number (Z^3) and Compton processes primarily dependent on electron density (Z^0). The atomic number of gadolinium, at 64, is greater than that of iodine at 53 which would suggest that it has the potential to provide greater absorption of x-rays, especially at energies exceeding the k-edge of gadolinium[29]. This

suggests that gadolinium containing compounds, especially the chelates that are currently in use clinically in MRI, could prove to be attractive contrast agents for CT especially if there are patients whose kidney function precludes the use of iodinated-contrast material but for whom gadolinium-based materials are not contraindicated. Patients with known allergic reactions to iodine could also benefit from the use of gadolinium-based agents. To date, several studies have been performed, with variable success, assessing the potential of gadolinium for use in clinical planar angiography and CTA[30-36].

1.1.3 Computed Tomography

The history of Computerized Tomography (CT) can be traced to the mathematical analytical tool of back projection developed by Radon in 1917[37]. By the late 1960's computer technology had sufficient power to take advantage of Radon's methods. In 1971 Hounsfield, working for the EMI Corporation, developed the first practical CT unit for imaging the human body[38]. Hounsfield developed an iterative method, which, with an 80X80 matrix, contained 6400 variables. Since he obtained a total of 28,800 projections this resulted in 28,800 simultaneous equations, thereby allowing for an optimum solution[38]. These pioneering units could only perform examinations of the head. For his efforts he was awarded the Nobel Prize in Medicine in 1979.

The original EMI unit utilized an x-ray tube and two NaI crystal detectors and therefore collected two sections at a time[39]. A third, reference, detector was in the beam before the patient[39]. The x-ray tube was typically operated at 120 kV and 30 mA with heavy filtration utilized to produce a spectrum that was less heterogeneous than the more lightly filtered beams commonly used in diagnostic radiological imaging. The beam was 3 mm wide (z-axis) and 13

mm long and the motion of the x-ray beam/detector assembly could best be described as translate/rotate. The assembly performed a linear translation across the anatomy with the x-ray beam on, stopped with the x-ray beam off, rotated 1 degree, and then repeated the process until it had rotated 180°. Each acquisition of two sections required approximately 5 minutes and an examination required approximately 25 minutes. It is interesting to note that the first commercial scanners used a convolution reconstruction method, patented by LeMay in 1976[40], which proved to be faster than that used by Hounsfield.

The next (second) generation of CT scanners utilized an array of detectors along the x-y axis of the patient (the z-axis being the long axis of the patient). The number of detectors varied with manufacturer with as many as 30 detectors being used by some. A fan beam intercepted the detector array. The motion of the system, like the first generation, was translate/rotate. By increasing the number of detectors and using a fan beam the rotation arc was increased from 1° to 30°, thus reducing the time per section to between 10 and 90 seconds[41].

Translational motion was completely eliminated with the introduction of the third generation of CT scanners. Third generation scanners utilize an array of several hundred detectors and a wide (approximately 50°) fan beam angle such that the axial section of patient is covered by the beam. The x-ray tube/detector array assembly rotated 360 degrees around the patient and stopped, the patient was then moved to a new slice location and the tube rotated 360 degrees in the opposite direction. This step and shoot condition was required because cables connected the rotating x-ray tube to the large heavy x-ray generator[38-42].

Some early third generation scanners utilized a pulsed x-ray beam while in others the beam remained on during the entire rotation. Data was acquired several times per second. As computer technology improved the sampling rate has continuously increased. This, combined

with higher output x-ray tubes and advances in mechanical engineering, has resulted in a decrease in the minimum exposure time from approximately 5 seconds per scan to less than 1 second per scan. This is the basic geometry used in modern scanners[38-42].

Fourth generation CT scanners utilized a 360° ring of detectors with the x-ray tube inside the detector ring and concentric with it. As with third generation units a fan beam is used. The advantage of this system was that it compensated for detector response fluctuations. Unfortunately the additional expense for detectors was prohibitive and as detector hardware improved, fluctuations became less of a problem. For these reasons, fourth generation scanning technology is not employed clinically and will not be considered in this work.

The introduction compact x-ray generators and slip ring technology in 1987[42] allowed the x-ray tube to rotate continuously about the patient[42]. Up to this point image data was acquired in a "step and shoot" manner as described; each axial tomographic section of anatomy was acquired at a fixed table position. The section was a two dimensional representation of anatomy perpendicular to the motion of the patient through the gantry and parallel to the rotational axis of the detector array. The development of slip ring technology made it possible to acquire a continuous volume of anatomical information by rotating the x-ray tube/detector array assembly while simultaneously moving the patient through the gantry. Concurrent with the development of slip ring technology was the increase in rotation speed of the x-ray tube/detector assembly and advances in x-ray tube design that allowed high heat loading and larger tube currents. Exposure times of less than 1 second per rotation became common. This was also facilitated by the development and use of high frequency generators. High frequency generators are lighter (they do not require an iron core) and smaller than the three-phase units that were used earlier. These

characteristics allowed them to rotate with the x-ray tube thereby allowing the slip ring to be operated at low voltage rather than at high voltage[42].

By the end of 1992 most of the major CT manufactures introduced spiral CT capability[42]. New terminology entered the lexicon of CT imaging: helical (also spiral) scanning and pitch. Helical scanning refers to the scanning dynamics of simultaneous table motion and x-ray tube/detector array rotation. Helical scanning provides volumetric data; transaxial images can be obtained at any point along the helix. Images are obtained by interpolation at either 180° or 360° points along the helix. The thickness of the transaxial image can be equal to or less than the collimated beam width. Pitch refers to the ratio of table incrementation to slice thickness. A pitch of 1:1 indicates that the table moves exactly the same distance per rotation as the width along the z-axis of the transaxial image. A pitch greater than 1:1 (eg. 2:1) indicates a gap whereas a pitch of less than 1:1 indicates overlap of image data. Overlapped data is very useful for constructing high quality 3-dimensional images. Pitches of greater than 1:1 provide a rapid acquisition of the volume imaged. Early helical scanners could perform a CT examination of the thorax in 40 seconds or less, depending on rotation time, pitch and collimation. Breath-hold CT examinations therefore became a possibility[38-42].

In 1998 General Electric, Marconi, Siemens, and Toshiba introduced multislice systems that employed four rows of detectors that could acquire 4 slices simultaneously. These systems, and all multi-row detector systems that followed, were third generation geometries[42]. Although it is possible to develop a fourth generation system with multiple rows of detectors, detectors had become more stable and the number of detectors needed would be quite large and not practical.

The development of multi-detector technology promoted the investigation of the utility of CT Angiography (CTA). The study of arteries requires the ability of the imaging system to

follow the course of transit of the radiopaque contrast media through the anatomy of interest rather quickly. A concurrent requirement is the ability of the imaging system to provide multi-planar and 3-D reconstructions from thin axial image data sets. In order to meet this second requirement with a minimum of artifacts thin, overlapping, axial image data is needed. These requirements could not be met with step-and-shoot systems and was difficult for single-row helical systems to meet. The first practical CTA system had 4 rows of detectors[39,41,42]. With this system 4 axial scans of thicknesses ranging from 1.25 mm to 5 mm could be obtained with each rotation of the x-ray tube/detector assembly. Exposure times as short as 0.6 seconds per rotation were possible. This translated to an ability to obtain 33.3 mm of continuous anatomic information per second with each axial image being 5 mm thick. Modern CT scanners employ as many as 320 rows of detectors to cover a large portion of anatomy (16 cm) in a single rotation[39,41,42].

1.2 Computed Tomography Dose

What follows is from a paper that was authored by Bonvento, Moore, and Olivieri-Fitt[43]. Patient radiation dose depends not only on the technical parameters employed but also the scanner geometry. To appreciate this, the radiation dose on 4-, 8-, and 16-multi detector computed tomography (MDCT) with both standard and near-identical techniques using thermoluminescent dosimeters (TLD) placed in or on an anthropomorphic Rando™ phantom (The Phantom Laboratory) [43].

The use of radiologic imaging, especially CT, has seen a significant increase over the past several years[44]. This increase in usage has raised the concern about radiation exposure and the health risks related to increased radiation exposure[45, 46]. Many studies have evaluated radiation

exposure in CT[47-51] and it was the topic of a consensus statement by the Fleischner Society, in which a suggestion of an appropriate radiation dose for CT of the chest was made[52]. A study performed in 1989 found that although CT accounted for only 2% of all radiologic studies, CT made up 20% of the effective radiation dose[53]. A follow-up study preformed several years later showed that both the use of CT and CT-related radiation exposure had doubled[54].

A standard range of radiation dose for multiple organs has been reported in several studies [52, 55-57]. Since the advent of MDCT, several studies have evaluated the radiation exposure between single-detector CT and MDCT[49, 52-53]. These studies have shown that there is an increase in radiation exposure of up to 27-36% with MDCT compared with single-detector CT. However, to date there has been no published study comparing radiation dose among the different available MDCT units. Groves et al. [58] compared the utility of a Monte Carlo-calculated radiation dose to thermoluminescent dosimeter-measured radiation dose and showed that the actual radiation dose was 18% higher than the calculated radiation dose with a 16-MDCT system.

1.3 Evaluation of Contrast Agents in Phantoms

The following is excerpted from a paper co-authored with W. Moore, T. Button, H Weismann, R. Yakupov, and A. Dilmanian[59]. The atomic number of gadolinium makes it suitable for CTA. The goal of this work is to quantify the potential of a gadolinium-based contrast agent (Gadovist, Schering AG, Berlin, Germany) compared to identical concentrations of an iodinated contrast agent (Conray, Mallinckrodt Inc., St. Louis, MO, U.S.A.) in terms of the contrast-to-noise ratio (CNR) in phantom CT studies. The rationale for this work is that the current state of x-ray radiography with iodinated contrast agents (which encompass all injectable radiography agents) is sub-optimal. First, these agents cause adverse reactions in large patient

populations, including those with allergies, asthma, kidney diseases, and diabetes[60-64]. The reactions can be severe or fatal. Second, iodine (Z=53) is not heavy enough to efficiently attenuate x rays at energies above 50 keV; gadolinium (Gd, Z=64), for example, is much better. Third, the filtered bremsstrahlung x-ray beams used are not ideal for contrast imaging in general, and Gd contrast imaging in particular, because they are very broad and have little intensity at the optimal energy above the K-edge of the contrast element.

A gadolinium-based agent may solve all these problems. First, because of its larger Z, Gd has a significantly larger attenuation coefficient for x rays > 50 keV than I. Consequently, its larger K-edge (50.23 keV for Gd vs. 33.17 keV for I) allows the use of x-ray beams with spectra concentrated just above the K-edge of the contrast element for general radiography with adequate transmission through the human body. Iodine cannot be used for similar purpose except for imaging thin body sections. Earlier imaging studies with phantoms and rabbits using monochromatic synchrotron x rays tuned above the K-edge of Gd, as well as the use of filtered x-ray beams imaged on a film-screen system, demonstrated some of the points indicated above[65].

1.4 Evaluation of Contrast Agents in Animals

This work was performed along with the phantom study described above[59]. Iodinated intravenous contrast media comprise all injectable x-ray radiography agents. The applications of these media have further increased since the recent development of computed tomography angiography (CTA) as a major imaging modality[18-21]. However, there are several shortcomings with the use of iodinated contrast media. First, it has potentially dangerous side effects, including hives, cardiac arrhythmias, renal failure, and anaphylactoid shock[22-23]. Second, iodine, with an atomic number of 53, is not adequately heavy to efficiently attenuate x-rays at energies higher

than about 50 keV, which comprise a major share of the beam energy spectra used in current CTA (commonly performed at 120 kVp or 140 kVp). Gadolinium, with its higher atomic number (Z = 64), attenuates these x-rays much more effectively for the same molar or gram concentrations of the contrast elements[29]. A challenge in modern radiology is to devise a new contrast medium that is safer and physically more suitable to the beam energy spectra used in the same image modality.

Gadolinium (Gd), a member of the lanthanide group of rare earth metals, has chemical properties that are suitable for producing a variety of chemical compounds, including those that can be safely used as contrast media. For this reason, and because of its adequate magnetic properties, Gd has been the basis for most magnetic resonance imaging contrast media, such as Magnevist and Gadovist[25]. Large-scale clinical studies have shown that these media, at doses used for clinical magnetic resonance imaging, have no significant detrimental effects on renal function even in patients with underlying renal insufficiency[25-26]. Because of Gd's larger atomic number than iodine, K-edge of 50.2 keV versus iodine's 33.2 keV, Gd produces a larger attenuation coefficient than iodine for x-ray energies higher than 50.2 keV[29].

To date, several studies have been performed, with variable success, assessing the potential of gadolinium for use in clinical planar angiography and CTA[30-36]. The purpose of the present study is to quantitatively compare the CT image contrast of Gd and iodine-based media in a rabbit model and in a phantom. Although the phantom studies provide physical information for this comparison, the rabbit studies indicate also physiologic factors.

1.5 The Contrast Agent Evaluation Model

The purpose of the contrast agent evaluation model is to develop a frame work for the evaluation of new and future contrast agents as they apply to CT. The model used will allow for analysis of potential agents and the impact of kilovoltage and filter combinations on image contrast and radiation dose. In this way the use of each agent may be optimized to provide the best image quality per unit radiation dose. A useful product of the contrast evaluation model is the minimum effective concentration (MEC) for a test contrast agent. This is the concentration of contrast agent required to produce a contrast-to-noise (CNR) of one per cGy radiation dose for a particular kV/filter combination in a cylindrical 16 cm water equivalent phantom containing a target with contrast agent.

The initial approach was to model the spectra from an x-ray tube at a specified kilovoltage. Next, the spectra was corrected to include the impact of any filtration. Projection data was then computed for a cylindrically symmetric solid water head phantom with a contrast-containing target at its center. Noise was applied to this resulting projection data based on photon counting statistics. In principle, standard filtered back projection could be applied providing a simulated image from which contrast-to-noise ratio (CNR) could be determined. In addition, the radiation dose at the center of the phantom was also computed from photon fluence providing the CNR per unit radiation dose.

Producing an accurate image from the projection data that was generated proved to be difficult. Matlab™ is capable of producing filtered backprojection images, but has several difficulties. First, the grey scale is only 8-bit. CT images consist of at least 2000 Hounsfield units (11 bits). Scaling the Matlab™ generated image to 11 bits proved to be impractical, at best.

There was also the difficult task of converting the .jpeg image into a DICOM image for analysis. Other difficulties included: selection of reconstructive filter, the use of a bowtie filters or other corrections of field uniformity. To avoid these difficulties we computed the contrast-to-noise ratio (CNR_p) of noisy projection data and then corrected for propagation of error and other errors using an empirically derived correction factor to obtain the contrast-to-noise ratio that would result in the reconstructed image (CNR_i).

Intuitively, as the size of the object increases its conspicuity will increase if the contrast and noise are held constant. One of the earliest investigators to attempt to quantify this was Albert Rose[77] whose works on the subject of visualization are widely quoted today some 70 years later. In this work, it was shown that for a series of circles whose diameter decreases by a factor of two moving from left to right and whose contrast decreases by a factor of two moving from top to bottom a diagonal line can be drawn from the upper right to the lower left demarcating visualized versus non-visualized objects. The diagonal will move to the right as the illumination (exposure) increases. Some useful conclusions can be drawn from these observations:

1. At constant contrast the size of an object that can be discerned is a function of the exposure.
2. At constant exposure the size of an object that can be discerned depends upon the contrast.
3. As exposure increases smaller objects of lower contrast can be discerned. In fact, a four-fold increase in exposure results in the smallest diameter object being reduced by a factor of two at any given contrast[77].

Rose's conclusions are quite useful but care must be taken when applying them to CT. First; the images that were used were created by light falling on objects and the reflected light was subsequently observed on a kinescope[77]. No image processing was employed. Second although the brightness and contrast levels of a kinescope can be adjusted this is not the same as selecting a threshold mid-range setting (level) and dynamic range (window) as is done in CT. Thirdly' the structure of noise in CT is a function of the reconstruction algorithm that is used. The Noise Power Spectrum (NPS) is used to characterize the frequency content of the noise. The frequency content will determine the size of objects that can be seen. For example, if the noise is the same size as the object of interest the object can be difficult or impossible to discern even if the actual noise figure implies otherwise (i.e., a Contrast to Noise Ratio, CNR, that would indicate good low-contrast discrimination).

An oft-quoted lower limit for detection of a low contrast pixel structure in a uniform background requires an SNR of five. This is based upon the work done by Rose and others that is discussed above. For the reasons that have been given this criterion is probably not appropriate for evaluating low-contrast performance in CT.

Using a target CNR_i of 1, the minimum effective concentration (MEC) of contrast agent can be computed per unit radiation dose. Using this parameter allows the study of the impact of kilovoltage and filtration and allows for their optimization. This contrast agent evaluation model can dramatically reduce empirical evaluation strategies using phantoms and animal models as described above.

2. Material and Methods

2.1 Contrast Agent Evaluation Model Components

The purpose of this work is to develop a frame-work for the evaluation of new and future contrast agents as they apply to CT. As described above, the initial approach will be to model the spectra from an x-ray tube at a specified kilovoltage, and compute the spectra that emerges

from the tube and ultimately from beneath a cylindrical phantom containing a contrast filled target as projection data. From these data image CNR_i can be determined as well as radiation dose allowing for computation of "minimum effective concentration". Methods for X-Ray Spectra From First Principles (2.1.1), X-Ray Spectra From SPEKTR (2.1.2), Solid Water Phantom (2.1.3), Generated image data (2.1.4) are described below.

2.1.1 X-ray Spectra From First Principles

Bremstraalung Radiation

In order to optimize the x-ray spectrum for any contrast media it is first necessary to develop a mathematical model of the x-ray generation process. Kim[66] and Storm[67] had carefully considered this problem in the past.

From Kim[66], the continuum energy intensity at photon energy k generated by an electron penetrating a distance in the target element is given by:

$$N_k = I_{A,k} * F_{B,k/Ti} * F_{C,k/Ti} * \exp(-\sum_i(u_i p_i x_i))dk/4\pi D^2 \quad (1)$$

Where N_k = number of photons/cm^2-sec in the energy interval k to k+dk per incident electron; $I_{A,k}$ = intensity of X-ray photons of energy k per incident electron; $F_{B,k/Ti}$ = backscatter factor; $F_{C,k/Ti}$ = target attenuation factor; k = photon energy in keV; T_i = initial electron energy in

keV; $\exp(-\sum_i(u_i p_i x_i))$ = attenuation due to filters of mass attenuation *u*, density *p*, and thickness, x; and D = distance from the target to the point of measurement in cm.

The contribution from characteristic radiation is not included in formula (1). (Characteristic radiation contribution will be discussed in the next section.)

Next, $I_{A,k}$ is considered[66]:

$$I_{A,k} = pN/A \int_k^{T_i} Q(dT/dx)^{-1}\, dT \quad (2)$$

Where N is Avogadro's number, *p* is the density of the target of interest, A is the atomic weight, dT/dx is the relative stopping power, and Q is the x-ray energy intensity per unit energy interval per incident electron flux per atom. The Q values have been obtained from Morin[68] and the stopping power data from the ICRU[69]. With this information, formula (2) can be re-written as follows[66]:

$$I_{A,k} = F_{A,k}(T_i - k) \quad (3)$$

where *k* is the photon energy, T_i is the electron energy and $F_{A,k}$ values for tungsten are given in table 1.

Photon energy, keV	$F_{A,k}$ X 10^{-4}
15	2.15
30	2.02
60	1.78
100	1.51
150	1.25
200	1.04
300	0.73

Table 1 - Intensity conversion factor ($F_{A,k}$) vs photon energy in keV[66]

A linear regression of these values produces:

$$F_{A,k} = (-6.77E\text{-}07 * E) + 2.21E\text{-}4 \quad (4)$$

where E is the photon energy in keV. The r^2 is 0.9904. Formula (3) can be easily used to generate spectra using standard spread sheets.

The target will attenuate radiation and a correction for this attenuation should be considered. Kim[66] uses the following correction:

$$F_{C,k/Ti} = \exp -[(f_{C,k/Ti}\, R_{W,Ti})u_{W,k}\, \cot\theta] \quad (5)$$

where $R_{W,Ti}$ is the continuously slowing down approximation (CSDA) range in g/cm^2 of an electron or energy T_i in tungsten, $f_{C,k/Ti}$ is the mean depth of production as a fraction of the CSDA range, $u_{W,k}$ is the mass attenuation coefficient in tungsten for photons of energy k, and θ is the tube angle in degrees. Values of $f_{C,k/Ti}$ versus k/T_i are given in table 2.

k/Ti	f(C,*k*/Ti)
0.1	0.12
0.3	0.11
0.5	0.1
0.7	0.09
0.8	0.08
0.9	0.05
1	0

Table 2 -Target attenuation factor vs fraction of electron energy that becomes photon energy[66]

An approximate formula for $f_{C,k/Ti}$ is given below which was also implemented in a spread sheet:

$$f(C, k/Ti) = 1.1E\text{-}01 + 1.6E\text{-}01(k/Ti) - 1.0\,(k/Ti)\text{^}2 + 1.9\,(k/Ti)\text{^}3 - 1.4(k/Ti)\text{^}4 + 1.6E\text{-}01(k/Ti)\text{^}5 \quad (6)$$

The CSDA range[70] is taken to range from 2.08E-02 g/cm^2 at 80 keV to 5.67E-02 g/cm^2 at 150 keV and the mass attenuation coefficient is taken to be 1.5(keV$^{-1.9}$) cm^2/gm. This is obtained

by graphing the following values for the mass attenuation coefficient for tungsten and performing a regression:

keV	u (cm^2/gm)
10	95.5
15	142
20	67
30	23
40	10.7
50	5.91
60	3.65
80	7.89
100	4.43
150	1.57

Table 3 - Mass attenuation coefficients of tungsten vs photon energy[16]

Characteristic Radiation

The total number of characteristic x-rays is given by: $5.1E11(E_0/E_k - 1)^{1.67}$ photons/sr-mAs[67], where E_0 is the k absorption energy of the target and Ek is the energy of the electron. Finally, 28.9% of the characteristics are at 58 keV, 50.8% are at 59 keV, 16.2% are at 67 keV

and 0.406% are at 69 keV[71]. Formulas 1 and 3 through 8 are quite amenable to use in a spreadsheet program such as Excel™ (Microsoft Corporation).

2.1.2 X-Ray Spectra From SPEKTR

Unfortunately the spectra that were generated using the methods developed by Kim described above did not model measured spectra particularly well. For example, methods of Kim did not predict exposure, exposure rate, or half-value layer satisfactorily as shown in the results section. For these reason, an alternate methods for generating spectra was required.

Tungsten Anode Spectral Model Using Interpolating Polynomials or TASMIP, as developed by Boone and Seibert[72], is a useful tool for the generation of x-ray spectra. It is, however, not very convenient to use. Siewerdsen, et.al.[73], developed a set of computational tools that make use of the TASMIP model but are much easier to use and that allow rapid modifications to the spectra that are generated.

SPEKTR is an adaptation of the TASMIP model to Matlab™ which is a very flexible and powerful computational tool. The toolkit is available as a free download from the American Institute of Physics includes a Graphical User Interface (GUI). The GUI allows the user to input the following parameters: kVp, waveform ripple, added filtration in millimeters of aluminum, additional filtration of a variety of elements and compounds, attenuation through thicknesses of water and other materials of imaging interest and the generation of spatial filters. The output is in photons per square millimeter per keV bin. The routine will calculate radiation intensity in mR/mAs at 100 cm distance, first through third Half-Value Layer (HVL) and Tenth-Value Layer (TVL), fluence per exposure and the mean energy.

The database used for attenuation contains mass and mass attenuation coefficients for elements 1 through 92 and for a variety of compounds. All of the data are from compilations of the National Institute of Standards and Technology. SPEKTR will generate spectra in 1 keV bins up to 150 keV and can be used from 15 to 150 kVp. The outputs are both graphical and tabulated. The Matlab™ matrix is easily converted to an Excel™ spreadsheet for further computational purposes.

Both TASMIP and SPEKTR were extensively validated by their respective developers. To assure proper SPEKTR use, spectra generated by SPEKTR were used to compute outputs and HVL's at various kVp's which were compared with measured results as described in the results section below. SPEKTR has been used exclusively for validation and use of the contrast agent evaluation model.

2.1.3 Solid Water Phantom

The acrylic phantom that was used for the preliminary testing of the models would not be acceptable for continuing the evaluation of the models that have been proposed. This is because acrylic does not mimic human tissue well as its CT number is much higher than most soft tissue (120 versus approximately 0). Since the anticipated CT number of the contrast material will be equal to or less than 120, depending on the concentration, the contrast between the phantom and the contrast material will be minimal if acrylic is used.

A phantom that mimics human tissue is needed for the evaluation of the radiographic contrast between a contrast-medium filled vessel and the surrounding soft tissue. There are several reasons for the choice of water. First; CT units are generally calibrated using water. The

CT number of water is calibrated to 0 for all kilovoltages, filters, fields of view, and slice thicknesses. In addition, water closely simulates soft tissue in its radiation attenuation characteristics because the effective Z of water is similar to the effective Z of soft tissue and the chemical makeup of water is similar to soft tissue. For these reasons water and water-equivalent solid materials have been used as the calibration medium for Radiation Therapy depth-dose calculations. Because water is abundant, easy to work with, and non-toxic, it has been used extensively in both Radiotherapy and Imaging.

It is important for the physical phantom that will be used for further validation of the model to be as close as possible to the simulated model as possible. A pure water phantom would be extremely difficult to use for validation purposes as the validation of the proposed procedure requires imaging vials of various concentrations of contrast media and measuring radiation exposure in the center of the phantom. For these reasons a solid phantom whose radiation interaction characteristics match those of water was deemed necessary. Based on the above considerations a phantom was designed and constructed of water-equivalent solid material. Since the American College of Radiology (ACR) specifies that CT dose index (CTDI) be measured in a 16 cm acrylic phantom the dimensions of the solid water phantom were based upon that phantom. The design parameters called for the phantom to be a cylinder 16 cm in diameter and 20 cm in length. Five holes run the full length of the phantom each being 1.5 cm in diameter. One hole is located in the center of the phantom and the remaining four are placed around the periphery of the phantom at the 12, 3, 6 and 9 o'clock positions with their centers 1 cm below the edge of the phantom. Rods of the same material as the phantom were designed to fit into the holes and run the full length of the phantom. This phantom design was submitted to Computerized Imaging Reference Systems, Incorporated (CIRS) for fabrication.

Upon receipt of the phantom the CT number accuracy was validated. CT imaging of the phantom was performed and the CT number of the phantom material was evaluated. The phantom was scanned on a General Electric Lightspeed 16™ CT scanner. Scans were performed at 80, 100, 120 and 140 kVp. The CT number of the phantom was measured near the center of the phantom (while avoiding the centrally located rod) using the workstation provided on the scanner. Scans of the GE supplied water phantom that is used for daily QC were also performed using the same parameters.

Figure 2 a and b – The CTDI Phantom (left) and the CIRS™ Solid Water Phantom (right)

2.1.4 Generated Image Data

With an appropriate spectrum, it is possible to generate CT projection data and use filtered backprojection to provide a computed cross sectional image. Dose in computed tomography is usually provided as a CT dose index (CTDI) representing the dose to standard phantom structures. Acrylic phantoms are used; one is a 16 cm diameter to simulate the head while the other is a 32 cm diameter cylinder to simulate the body. Both are 16 cm in length. For the purpose of evaluating contrast agents, the CTDI head phantom structure will be employed

using water equivalent plastic rather than acrylic as described above. For this initial image formation, however, acrylic was used.

From a computed spectrum, it is possible to project individual rays through the cylinder center and calculate the number of photons at each keV interval that reach individual detectors. For each keV bin the spectrum data provides the number of photons per square millimeter at a given distance. Differential absorption will, of course, be a function of the thickness of acrylic transversed which is found by treating each ray separately. For the 16 cm diameter phantom the path length will vary from 0 to 16 cm. All specifications are from the product data sheet for the General Electric Lightspeed CT unit[74]. The rays project from the focal spot and the total fan angle is 55 degrees. There are a total of 888 detectors. The focus to isocenter distance is 54 cm and 8 cm must be added beyond the center to account for the full diameter of the phantom. The fan angle that subtends the phantom is 0.298 radians and this, in turn, subtends 282 detectors. Since the geometry is symmetrical about the center a total path length for 141 rays needs to be calculated. Simple trigonometry yields the path length for each ray. This length, in turn, is multiplied by the linear attenuation coefficient for acrylic for each energy and the result obtained is used to calculate the attenuation experienced by each ray.

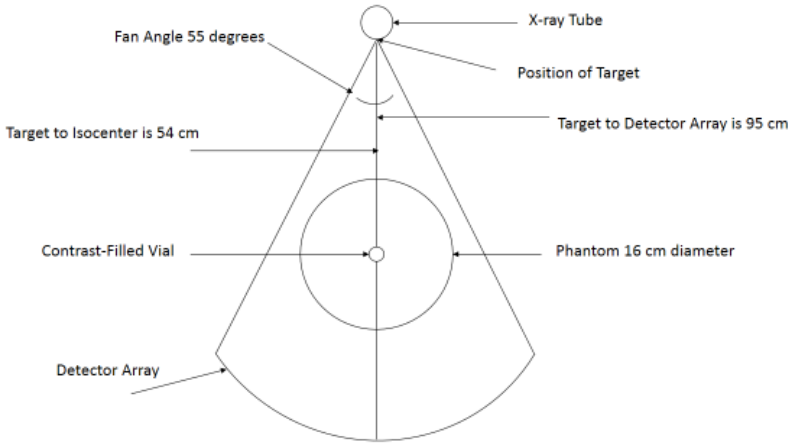

Figure 3 – Diagram of the Geometry of the X-ray Tube, Phantom and Detector

Targets containing prototype contrast agents may also be incorporated, most appropriately at the phantom center. The result is a simple projection of the object. The events that will actually be detected will follow Poisson counting statistics. These statistics may be incorporated into each projection by employing a Poisson random numbers generator based on the events observed at each detector to generate a noisy complete projection set. With this noisy projection data it is then possible to perform filtered back projection to generate a pseudo image of the phantom.

The CT tube used to model the x-ray spectrum is based upon the General Electric Lightspeed™ 16 CT unit with a Performix™ x-ray tube assembly. The stated filtration for this insert, tube housing, and collimator assembly is 5.65 mm Al equivalent. This unit has a focus to detector distance of 95 cm and a focus to isocenter distance of 54 cm. The fan angle is 55 degrees. There are 888 patient elements and 24 reference elements[74.] The detector arc is 0.96 radians and this produces an element size of 0.1 cm. The detectors are arranged in an arc that

fully subtends the 55 degree fan beam which results in an arc that is 91 cm in length. The active area is a 0.625 mm square. There are 16 rows of detectors along the long (Z) axis of the patient.

At isocenter plus 8 cm the arc of the fan is 59.5 cm. The fan angle subtended by the 16 cm phantom at isocenter is 0.298 radians. This means that 282 individual rays pass through the phantom to the detectors. Matlab was used to calculate 360 separate projections, each one with Poisson counting statistics applied using a random number generator that applies a random number to yield the probability that the actual number of photons will be within +/- 3 standard deviations of the predicted number of photons. The standard deviation is assumed to be the square root of the predicted number of photons. The random number generator yields values of 0 to 1. Numbers less than 0.5 yield a figure less than the predicted number and greater than 0.5 yield a higher number. At 0.5 the number is exactly the predicted number. The Poisson Distribution is appropriate for counting large numbers of events[83]. The probability of observing k events in an interval is given by:

Equation 7

$$P(k) = \frac{\lambda^k e^{-\lambda}}{k!}$$

Where:

λ = the average number of events in the interval

k = an integer (0, 1, 2…)

k! = the factorial of k

e = Euler's number

The distribution for large numbers is characterized by the standard deviation (σ) being equal to the square root of the mean number of counts.

$$\sigma = x^{1/2} \quad (8)$$

Where σ is the standard deviation of the mean x.[83]

Finally, filtered backprojection, using a simple ramp filter, was applied to the 360 noisy projection data sets to produce a simulated image.

2.2 Measured Radiation Dose in Computed Tomography

In the Comparison of MDCT Radiation Dose: A Phantom Study[43], radiation dose was measured for a multislice CT in a Rando phantom using thermoluminescent dosimeters. Before all experiments, a total of 60 thermoluminescent dosimeters were annealed at 400°C for 2 hours, then at 100°C for 1 hour. Using a male Rando™ anthropomorphic phantom, five thermoluminescent dosimeters, wrapped in cellophane, were placed into the predrilled hole at the center of slice 18 of the phantom (near the center of the heart). Additional packages of five thermoluminescent dosimeters were affixed, with silk tape, to the anterior and lateral aspects of the phantom of slice 18, at the level of the heart in the lower chest (Figure 2). All thermoluminescent dosimeters were kept in small opaque packages to minimize the effects of exposure to ambient light.

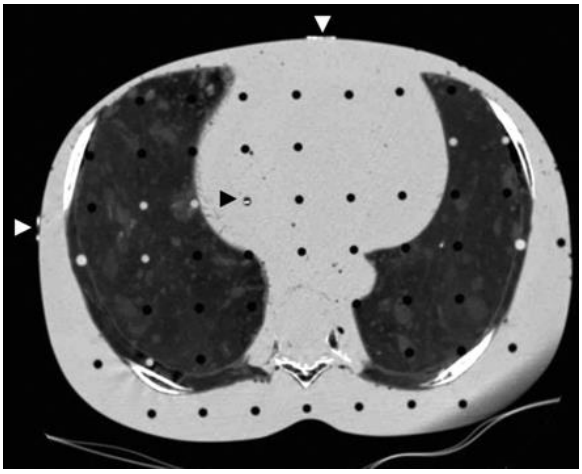

Figure 4 —Axial CT image of chest at section 18 of Rando phantom (The Phantom Laboratory). Packets of thermoluminescent dosimeters wrapped in cellophane (*arrowheads*) are placed at anterior, lateral, and center positions in this slice[43].

The anthropomorphic phantom was placed on the CT table and a standard departmental protocol CT of the chest was performed using SMART mA™ SMART mA™ is a proprietary algorithm of GE Healthcare™ that modulates the tube current (mA) exclusively on the *z*-axis based on patient habitus and an operator-selected image-quality specification (Noise Index™, GE Healthcare™). Specific protocols are detailed in Table 4 and were as follows: LightSpeed 4™ (GE Healthcare™): detector array, 4 x 2.5 mm; field of view, 36 cm; table speed, 15 mm/s; rotation time, 0.6 seconds; 120 kVp; pitch, 1.5:1; and noise index, 11 (the noise index refers to the reference standard deviation of a homogeneous region towards the center of the anatomy that is imaged. Tube current modulation is performed by the CT unit to achieve the user selected

noise index). Light-Speed 8™: detector array, 8 x 1.25 mm; field of view, 36 cm; table speed, 13.5 mm/s; rotation time, 0.6 seconds; 120 kVp; pitch, 1.35:1; and noise index, 10.4. LightSpeed 16™: detector array, 16 x 1.25; field of view, 36 cm; table speed, 27.5 mm/s; rotation time, 0.6 seconds; 120 kVp; pitch, 1.35:1; and noise index, 11.5. All exposures were performed with SMART mA™.

Parameter	Scanner		
	4-MDCT	8-MDCT	16-MDCT
Detector Configuration	4 x 2.5	8 x 1.25	16 x 1.25
Field of View (cm)	36	36	36
Table speed (mm/sec)	15	13.5	27.5
Pitch	1.5:1	1.35:1	1.35:1
Nominal prepatient collimation	10	10	20
Actual prepatient collimation	13	13	21
mA	243	251	265
Noise index	11	10.4	11.5
DLP/ED	366/12.2	505/16.8	359/12.0
Note - mA refers to the mA chosen by SMART mA (GE Healthcare) at slice 18 of the phantom.			
DLP = dose-length product in milligray x cm, ED = effective dose in millisieverts.			

Table 4 – Parameters for standard departmental chest CT (from previously co-authored publishcation[43]).

The second experiment was performed using near-identical techniques[43]. Specific protocols are detailed in Table 5 and were as follows: Light-Speed 4™: detector array, 4 x 1.25 mm; field of view, 36 cm; table speed, 7.5 mm/s; rotation time, 0.6 seconds; 120 kVp; pitch, 1.5:1; noise index, 13. LightSpeed 8™: detector array, 8 x 1.25 mm; field of view, 36 cm; table speed, 13.5 mm/s; rotation time, 0.6 seconds; 120 kVp; pitch, 1.35:1; noise index, 13.

LightSpeed 16™: detector array, 16 x 1.25; field of view, 36 cm; table speed, 27.5 mm/s; rotation time, 0.6 seconds; 120 kVp; pitch, 1.35:1; noise index, 11. All exposures were performed with SMART mA™. The noise index was chosen based on the SD in the Rando™ phantom's heart in each CT unit. The Standard Deviation was set to approximately 8 HU for all three scanners. The table speed in the 4-detector unit is the maximal speed allowed in this unit at 4 x 2.5 mm.

Parameter	Scanner		
	4-MDCT	8-MDCT	16-MDCT
Detector Configuration	4 x 1.25	8 x 1.25	16 x 1.25
Field of View (cm)	36	36	36
Table speed (mm/sec)	7.5	13.5	27.5
Pitch	1.5:1	1.35:1	1.35:1
Nominal prepatient collimation	5	10	20
Actual prepatient collimation	8	13	21
mA	373	245	257
Noise index	13	13	11
DLP/ED	575/20	522/17.4	432/14.4
Note - mA refers to the mA chosen by SMART mA (GE Healthcare) at slice 18 of the phantom. DLP = dose-length product in milligray x cm, ED = effective dose in millisieverts.			

Table 5 – Parameters used to create near-identical chest CT technique (from previously co-authored publishcation[43]).

Before interpreting the thermoluminescent dosimeters, a 24-hour waiting period was observed to allow electrons in short lived states to return to low energy. This has been shown to decrease the number of outlier measurements[51]. The thermoluminescent dosimeters were then interpreted using a Model 3500™ thermoluminescent dosimeter reader (Harshaw Chemical), and the output of the reader was recorded in nano-coulombs (nC). After each set of exposures, a

separate set of thermoluminescent dosimeters were exposed to known levels of radiation. Calibration was performed using an electron chamber (MDH RadCal™). Three separate exposures were made: 11.3 mGy (94.4 nC), 22.4 mGy (201.1 nC), and 45.0 mGy (331.5 nC). These thermoluminescent dosimeters were also interpreted 24 hours after exposure, and conversion of nanocoulombs to grays was generated. This was used to calculate radiation dose for the remaining thermoluminescent dosimeters, which were placed in or on the Rando phantom.

2.3 Evaluation of Contrast Agents in Phantoms[59]

The following is excerpted from a paper co-authored with W. Moore, T. Button, H Weismann, R. Yakupov, and A. Dilmanian[59]. All studies used a General Electric Lightspeed CT™ unit (GE Medical Systems™, Milwaukee, WI) of the Department of Radiology, State University of New York, Stony Brook. No attempt was made to alter the spectra of the x-ray beams with additional beam filtration. The image analyses were carried out using a Radworks™ workstation (General Electric Medical Systems™).

Commercially available Magnevist™ (0.5 molar Gd-dimeglumine, Berlex Laboratories, Montville, NJ) and Ultravist 300™ (2.4 molar iodine Schering AG, Germany) were diluted to 25, 40, 50, and 300 mmole, and 35, 50, 100, and 320 mmole of the contrast elements, respectively. All dilutions were performed with 3× normal saline to simulate the CT attenuation of blood. Clear plastic vials containing each of the above concentration of iodine or Gd were placed into the center of an acrylic 32-cm diameter cylindrical CT body phantom (Nuclear Associates™ 76-415) for individual studies. Three separate axial acquisitions were obtained at 80, 100, and 120 kVp using a 50-cm field of view for each molar concentration. All acquisitions

were obtained using 300 mA and a rotation time of 0.8 seconds. In each set of the acquired images, the attenuation of the x-ray beam was measured in three different axial regions of the vial.

2.4 Evaluation of Contrast Agents in Animals[59]

The following is excerpted from a paper co-authored with W. Moore, T. Button, H Weismann, R. Yakupov, and A. Dilmanian[59]. The rabbit studies were approved by the Institutional Animal Care and Use Committees at the State University of New York, Stony Brook. Three separate experiments were performed on a 7-kg Giant Flemish rabbit, each separated by at least 1 week. The helical CT parameters were as follows: field of view of 25 cm; rotation time of 0.5 seconds; slice thickness of 2.5 mm; pitch of 1.675:1; and table speed of 33.5 mm/rotation. At each time point after the completion of the injection of the contrast media, three back-to-back images were obtained at 80, 100, and 120 kVp in this order, each series taking approximately 6 seconds.

Experiment 1[59]

A total volume of 20 mL of Gadovist™ (1.0 molar gadolinium DTPA, Schering AG) was manually injected into the rabbit's ear vein using a 20-gage intravenous catheter. The injection took approximately 15 seconds to complete. The first set of images was acquired approximately 10 seconds after the completion of the injection; the imaging was repeated at 5 and 10 minutes after the injection of the contrast media. Each imaging set included 80, 100, and 120 kVp, using 400, 350, and 245 mA tube currents, respectively.

Experiment 2[59]

A total volume of 20 mL of Ultravist 300 was manually injected, in about 15 seconds, in the rabbit's ear vein via a 20-gage intravenous catheter. Imaging was initiated after an approximate delay of 10 seconds, and repeated at 5 and 10 minutes after the injection of the contrast media. Each set of imaging included 80, 100, and 120 kVp, all using a 200 mA tube current.

Experiment 3[59]

Using dosages of gadolinium shown to be safe in human trials[24,25] (0.3 mg/kg) we administered 6 mL of Magnevist (0.5 molar gadolinium DTPA; 2.0 mL/mg), which for a 7-kg rabbit, amounted to about the same 0.3 mg/kg. As in the prior experiments, the agent was administered via a 20-gage intravenous catheter into an ear vein of the rabbit by manual injection in less than 5 seconds. A 5-mL flush of normal saline was injected by a parallel port immediately after the injection of gadolinium to clear the gadolinium from the intravenous tubing. Identical imaging protocols were used as described in Experiment 2. No 10-minute images were obtained for this experiment because the contrast enhancement was felt to have mostly washed out at 5 minutes.

2.5 Evaluation of Iodine and Gadolinium Using the Contrast Agent Evaluation Model

An initial aspect of validating the contrast agent evaluation model was to evaluating the x-ray spectra generated by SPEKTR. In addition to examining the generated spectra, it was also important to assure that the half value layer (HVL), output and CT numbers derived from SPEKTR matched a real CT x-ray system. The x-ray spectra validation employed comparison with a GE Light Speed Ultra[16]™ Performix™ x-ray tube (Milwaukee, WI) operating at 120 kVp. The SPEKTR generated spectrum is

based upon 120 kVp with 3.9 mm aluminum added to the inherent 1.1 mm for a total of 5.0 mm, plus 0.002 mm of tungsten inherent filtration.

Next projection data was computed and a pseudo image was formed that simulated a 16 cm water phantom containing a contrast agent filled target. The target was 1.0 cm diameter to simulate a large vessel and was located in the center of the phantom. Various types and concentrations of contrast agent could be simulated for any kilovoltage and/or filter combination. The CNR_i provided by the target using the contrast agent evaluation model was compared directly to CT images acquired using the GE Light Speed Ultra scanner.

Finally, based on the calculated the photon fluence, the expected radiation dose could also be computed by including attenuation through half the solid water equivalent head phantom (8 cm) and then empirically correcting for scatter. This calculated dose could be compared to that directly with that measured in the solid water phantom.

2.6 Determining CNR_i using the Contrast Agent Evaluation Model

Since SPEKTR generated spectra can be used to generate projection data, a theoretical image can be computed and image contrast-to-noise ratio (CNR_i) of a contrast agent-containing target in a solid water phantom can be directly computed. Unfortunately, as previously described, the details of image generation have a variety of problems that make it difficult to assess CNR_i. To avoid these difficulties, the contrast- to-noise ratio of noisy projection data (CNRp) was computed and then corrected for propagation of error and additional errors using an empirically derived correction factor. The correction factor was determined by first calculating the CT number and the noise for 0.5, 5.0, and 50 mM of Gd at 120 kVp and 350 mAs. The noise

was calculated by using the square root of the intensity for each detector as the standard deviation, applying a random number that varies between 0 and 1 as the probability for the normal distribution function and then calculating the expected signal at the detector which is the mean intensity with the square root added or subtracted depending upon the value of the random number that was generated. The standard deviation of 20 iterations of calculating the mean of the detectors immediately surrounding the contrast-filled section was calculated. The standard deviation is then the noise. The CNRp is the CT number of the contrast-filled section divided by the calculated noise.

The CNRi is found by obtaining regions of interest from the contrast-filled vial and the surrounding phantom from images that were acquired on the clinical CT unit using

the same conditions (120 kVp, 350 mAs) used for calculating the CNR_p. The CNRi is then the difference of the CT number of the contrast-filled vial and surrounding phantom divided by the standard deviation (in Hounsfield units) of the region of interest adjacent to the contrast-filled vial. The correction factor is the CNR_i/CNR_p.

The calculations for determining the CT number in the projection data are shown below:

$$\boldsymbol{Az = -ln\left(\frac{Sc}{Se}\right)\ when\ the\ center\ is\ filled\ with\ 1\ cm\ diameter\ of\ Z\ solution}\ (\mathbf{9})$$

$$\boldsymbol{Aw = -ln\left(\frac{Sc}{Se}\right)\ when\ the\ center\ is\ filled\ with\ 1\ cm\ diameter\ of\ water}\ (\mathbf{10})$$

$$\boldsymbol{uw = \frac{Aw}{16}}\ (\mathbf{8})$$

$$\boldsymbol{uz = (Az * 1(cm) - 15(cm) * uw)}\ (\mathbf{11})$$

$$\boldsymbol{CT\#\ of\ target = 1000 * \left(\frac{uz - uw}{uw}\right)}\ (\mathbf{12})$$

Where:

A = the attenuation of the material in question at the center of he phantom.

S = the signal (number of photons per mm^2 at the detector * the energy of each photon).

u = the linear attenuation coefficient of the material in question.

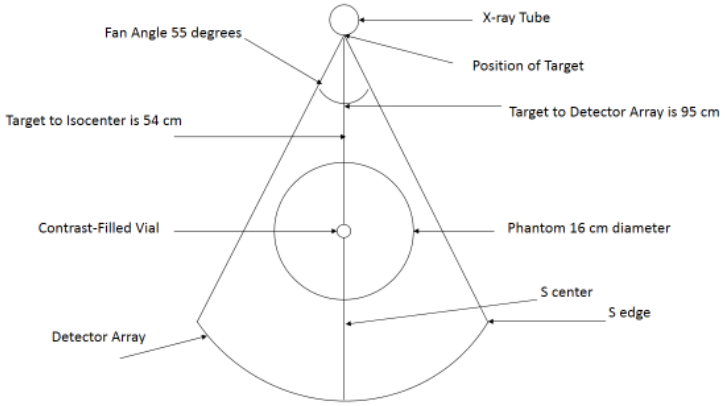

Figure 5 – Geometry for Calculating Contrast and CNR

In order to take account of the random nature of photon production and subsequent absorption by the detectors a random number generator was applied to the number of photons reaching the detectors adjacent to the center of the phantom. The number of photons reaching each detector is multiplied by a random number generated using a normal distribution function that is based upon the square root of the number of photons that was calculated to reach the detector. The intensity is found by multiplying the result by the energy of each photon. The CT number of the result is then calculated for the two detectors just prior and just after the central target location and the absolute value of the mean of these detectors are taken. The CT number of the standard deviation is calculated using the same set of formulas provided above except the standard deviation of the mean of the randomly generated values replaces signal (S). The projection CNR_p is calculated by dividing the CT number for the material in question by the CT number of the standard deviation (noise). The empirically derived correction is simply the ratio these two CNR_p divided by CNR_i.

2.7 Dose

The dose to the center of the solid water phantom was estimated using SPEKTR at various kVp and filter combinations. To accomplish this the exposure to the phantom was measured at various kVp's and compared to the exposures predicted by SPEKTR.

All measurements were made using the General Electric Lightspeed® CT scanner operated at 100 mA and 1 second rotation time. The total collimation was set to a nominal 20 mm (two 10 mm wide images). An MDH AccuPro® dosimetry system was used with a 10X5-0.6 chamber. The chamber was placed in the center hole of the phantom and centered in the beam. The phantom was placed in the isocenter of the gantry. Measurements were also made in air to determine the accuracy of the SPEKTR estimates without scattering media. For the in-air measurements the chamber was placed at the isocenter of the gantry.

SPEKTR was used to generate spectra for analysis. Spectra were generated at 80, 100, 120, and 140 kVp. The inherent filtration of SPEKTR is 1.1 mm of Al; 3.9 mm Al plus 0.002 mm of W were added to the inherent filtration. Ripple was assumed to be 0%. The Performix x-ray tube/housing/collimator assembly has 5.65 mm of Al equivalent (at 70 kV) permanently in the path of the beam (GE Medical Systems Lightspeed[16]. The paper by Siewerdsen, et.al.[73] recommends the addition of 0.002 mm of tungsten to the TASMIP model to account for target thickness

Exposure was determined from photon fluence at each energy and attenuation of 8 cm applied to compensate for phantom attenuation. The Graphical User Interface provides exposure (mR/mAs) for a variety of filters and absorbers. Because the GUI does not compensate for scatter, measured exposures were used to calculate the correction factor needed to compensate for the contribution of scatter. To correct for scatter, the ratio of the measured exposure to the

predicted exposure was used. The correction factors are kVp dependent are: 2.16, 2.06, 1.94, and 1.91 for 80, 10, 120, and 140 kVp, respectively. The calculated exposure for each kVp was multiplied by the correction factor to obtain the predicted exposure in the phantom at the 8 cm depth. Finally, a conversion factor of 0.009 mGy/mR was used to convert exposure to dose.

2.8 Assessing Contrast Agent Effectiveness

As described, in CT the ability to discern objects whose attenuation is close to the attenuation of the surrounding tissue depend primarily on: the difference in attenuation (contrast), the variation in calculated attenuation (statistical noise), and the size of the object. The difference in attenuation is, by definition, the difference in Hounsfield Units (CT#). The statistical difference in CT#'s in the background is the noise that limits the ability to discern objects when the contrast between the objects of interest and the surrounding area is small.

For the purpose of evaluation of contrast agents, it is important to determine the minimum concentration that will render isointense anatomy detectable per unit radiation dose. The selection of contrast-to-noise value required for detection is somewhat arbitrary. The American College of Radiology CT phantom has low contrast structures which are scored for detection based on a contrast-to-noise ratio (CNR) of approximately 1. This seems a reasonable base line. Therefore, for this work we will determine contrast agent concentration required for detection with a CNR of 1 per unit dose delivered.

Methods are provided to compute CNR_i as described in section 2.6. CNR_i is found from image data that were generated using the water-equivalent plastic phantom with a vial containing contrast material located in the center of the phantom. Regions of Interest were drawn in the

center of the vial and in an area of the phantom adjacent to the vial. The CNR_i is the contrast between the contrast material and the surrounding area divided by the standard deviation of the ROI in the surrounding area. Calculation of radiation dose is described in section 2.7 for a target in the center of a 16 cm phantom. The exposure that is calculated by SPEKTR is multiplied by the correction for scatter that was computed for the kVp used and the dose is found by multiplying this result by 0.009 mGy/mR or 0.0009 rad/mR.

Using a target CNR_i of unity, the fact that contrast is proportional to contrast agent concentration and CNR is proportional to the square root of dose, it is possible to compute the Minimum Effective Concentration (MEC). First, it is necessary to find the mAs at the test kVp that will yield a dose to the center of the phantom of 1 rad. Next, the noise that results in the center of the phantom at this mAs can be found. The number of photons reaching each detector is multiplied by a random number generated using a normal distribution function that is based upon the square root of the number of photons that was calculated to reach the detector. The intensity is found by multiplying the result by the energy of each photon. The CT number of the result is then calculated for the two detectors just prior and just after the central target location and the absolute value of the mean of these detectors are taken. The CT number of the standard deviation is calculated using the same set of formulas provided above (6 – 10) except the standard deviation of the mean of the randomly generated values replaces signal (S).

3. Results

3.1 Contrast Agent Evaluation Model

3.1.1 X-Ray Spectra From First Principles

X-ray spectra were calculated using the method described by Kim[66] above. This First-Principles method was thought to be a reasonable approach to generating spectra for application to the contrast evaluation model. As will be seen, the inaccuracies that resulted from its use precluded its use and SPEKTR was used for the conclusive work of this project. The inclusion of this data is provided in order to demonstrate the rationale for the use of SPEKTR.

The output spectrum for an x-ray operating at 120 kVp_{cp} with the electrons incident on a 17° tungsten target filtered with 4 mm Al and evaluated at 75 cm from the target is shown in Figure 3. The spectrum is in 1 keV steps. Integration of the spectra provides the total number of photons per square centimeter at 75 cm. In this case, integration gives 6.18 X 10^8 photons per square centimeter.

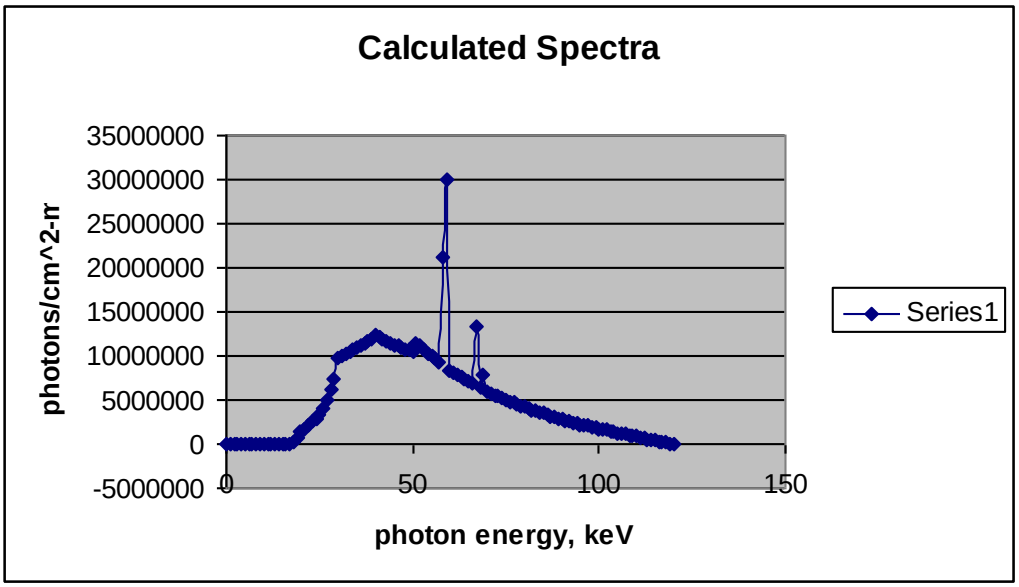

Figure 6 – Calculated spectrum (photons per cm^2 per mAs) at 75 cm from a tungsten target x-ray tube operating at 120 $kVp_{cp.}$ The anode angle is 17 degrees and 4 mm Al filtration.

Figure 7 is the spectra measured by Birch, Marshall and Ardran under the same conditions (kVp, target-evaluation distance, target angle, and filtration)[17]. The total number of photons measured was 6.29 X 10^8 photons per square centimeter per mAs at 75 cm. The agreement between the computed and measured total photons per square centimeter per mAs is within 2%.

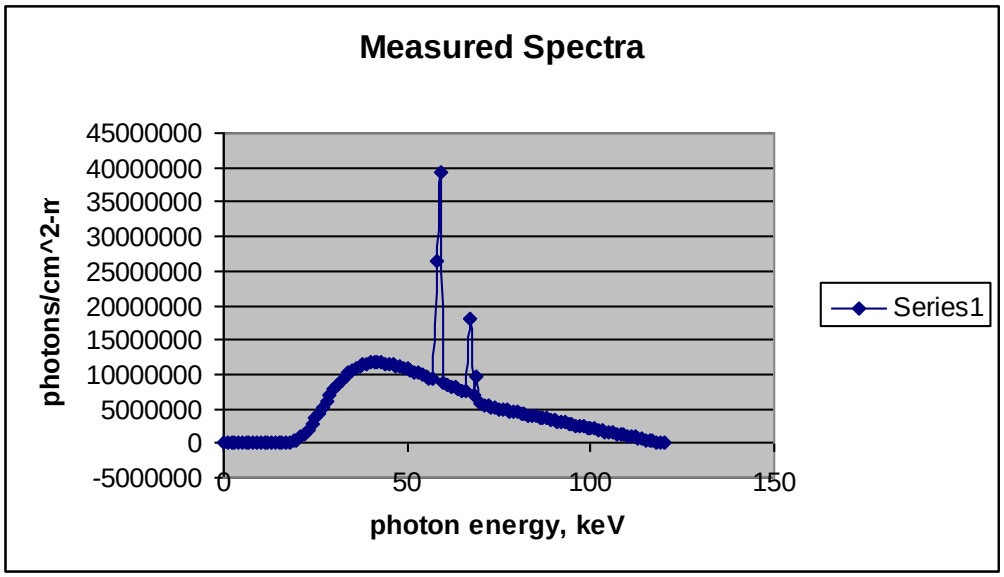

Figure 7 – Measured spectrum (photons per cm^2 per mAs) at 75 cm from a tungsten target x-ray tube operating at 120 $kVp_{cp.}$ The anode angle is 11degrees and 4 mm Al filtration.

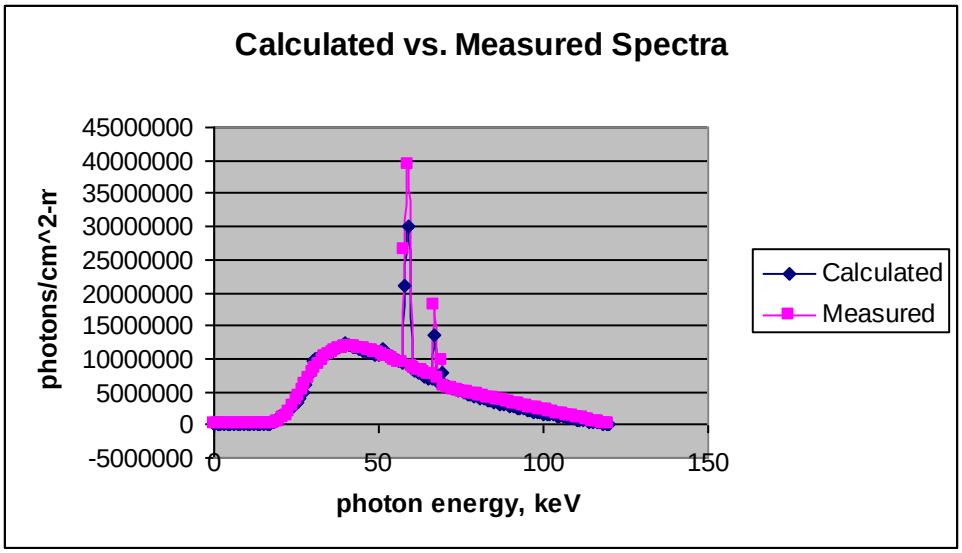

Figure 8 – Calculated vs Measured Spectra

Finally, figure 8 is a direct point by point comparison of the calculated and measured spectra. Even though the total numbers of photons per square centimeter are within 2% of each other, some important discrepancies are apparent. First, the calculated number of photons

between 16 and 21 keV is far greater than measured by Birch, ranging from a factor of 6 at 16 keV to 2 at 21 keV. Next, the calculation appears to underestimate the number of characteristic photons. At 67 keV the maximum discrepancy of 24% occurs and a minimum of 18% at 58 keV. Finally, from 95 keV to 120 kev the calculated number of photons per square centimeter is some 20% less than measured.

Measurements were made on a General Electric general-purpose radiographic/fluoroscopic unit located in the Radiology Department at Stony Brook University Hospital. The X-Ray tube is a General Electric model MX100. Measurements were made at 80, 100, and 120 kVp. Comparisons were made between calculated output (mR/mAs) using Kim and measured output. The HVL was not estimated using Kim. Kim overestimated the output by 39%13%, and 28%, respectively.

The discrepancy between calculated and measured spectra at low energies could very well be due to ignoring the effect of the glass and oil in the x-ray tube housing in the calculation of the spectrum. As these low energy photons are not anticipated to have much of an effect on the final image they can be safely ignored. The discrepancies at higher energies and in the characteristic portion of the spectrum are more difficult to understand. Others have experienced a similar difficulty. Storm[67] considered an agreement of 20% to be acceptable and concluded that the accuracy of characteristic modeling is dependent upon the accuracy of the Bremsstrahlung model. Tothill[74] also found that measured k-characteristic spectrum exceeded the theoretically derived spectrum. Nickoloff and Berman Found that the shape of the accelerating voltage waveform affected the shape of the resulting spectrum[76].

The discrepancies noted above between computed and measured spectra and measureable parameters using Kim lead to further consideration of improved modeling techniques and the application of SPEKTR[73]. The results obtained with SPEKTR are described below.

3.1.2 SPEKTR Generated Spectra

SPEKTR was used to generate spectra in order to estimate the output and HVL of a clinical radiographic unit. This was done primarily to validate the utility and flexibility of SPEKTR. These measurements were made on a general-purpose radiographic unit located in the Radiology Department at Stony Brook University Hospital (Toshiba DRX3724HD X-Ray Tube). The comparison of predicted and measured half value layer (HVL) in mm Al and output in mR/mAs is shown in Table 6. The agreement between predicted and measured half value over the range of kilovoltages used clinically for CT (80 – 140 kVp) is typically better than 5%. The agreement between predicted and measure output over the clinically relevant range is typically better than 7%. Agreement between measured and computed (SPEKTR) HVL and output results are excellent and SPEKTR generated data will be suitable in testing the contrast agent evaluation model. Figure 9 is the SPEKTR generated spectrum used for modeling the CT tube at 120 kVp.

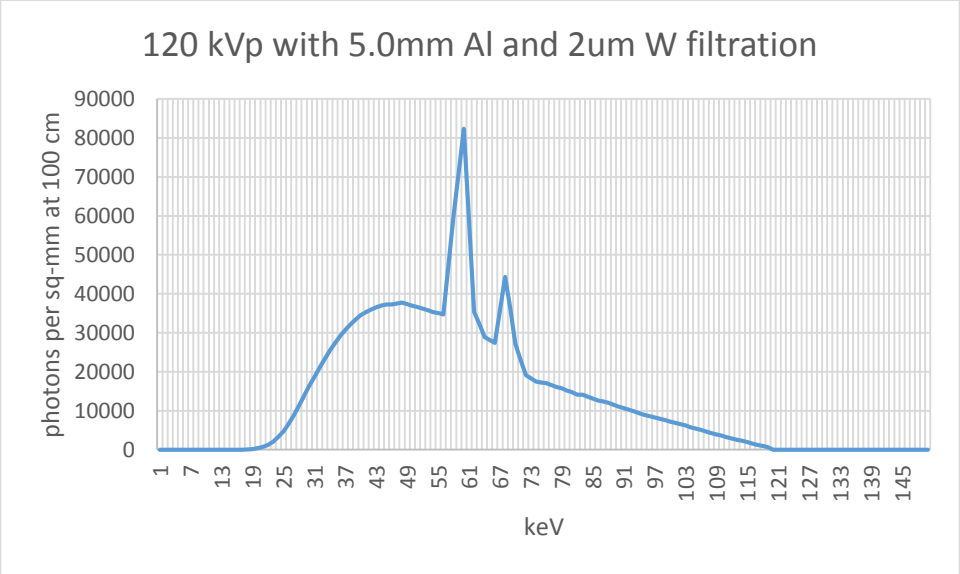

Figure 9 SPEKTR generated spectrum at 120 kVp with 5.0 mm total Al filtration and 2*u*m W filtration added

kVp	HVL Predicted	HVL measured	% Difference	mR/mAs Predicted	mR/mAs Measured	% Difference
80	3.15	2.99	5.08%	6.27	6.71	-7.02%
100	3.91	3.85	1.53%	9.80	10.1	-2.86%
120	4.64	4.65	-0.22%	13.8	13.6	1.45%
140	5.29	5.50	-3.97%	18.2	18.1	0.66%

Table 6 – Comparison of measured and computed (SPEKTR) output and HV

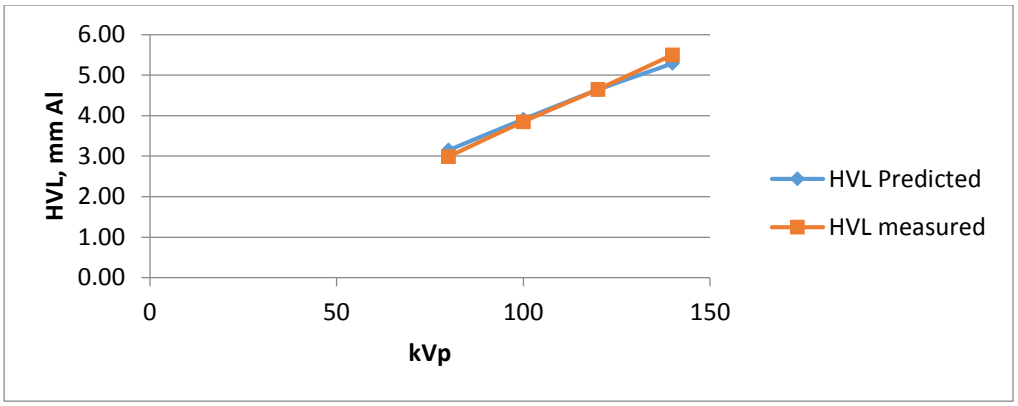

Figure 10 – Graphic comparison of mesured and computed (SPEKTR) HVL.

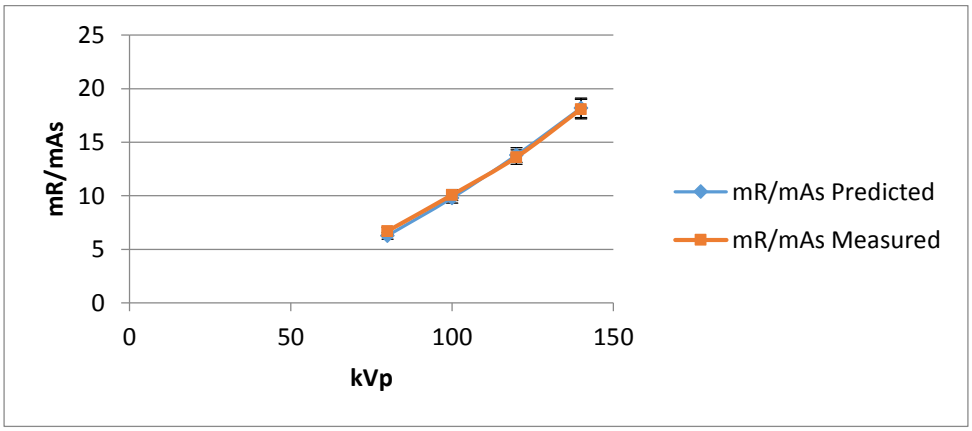

Figure 11 – Graphic comparison of measured and computed (SPEKTR) output.

Next SPEKTR spectra was generated based on the General Electric Lightspeed Ultra CT™ scanner that is employed for testing the contrast agent evaluation model. SPEKTR spectra were generated at 80, 100,120 and 140 kVp, with 0% ripple, 0.002mm tungsten and 3.9mm aluminum added filtration (which yields 5.0mm of aluminum with the inherent 1.1mm). The choice of filtration was based on the result of several attempts to accurately match the measureable characteristics of the General Electric Performix x-ray tube (output and HVL). The

addition of 2μm W was suggested by Siewerdsen[73] to compensate for the thickness of tungsten in the target. Exposures were calculated at 100 cm in air for 100 mAs and compared to measured exposures. An MDH/RADCAL AccuPro™ Dosimetry system with an MDH/RADCAL 10x5-0.6 (0.6 cc) chamber was used. Agreement between the predicted and measured exposures was excellent, ranging between 2.76 and 7.31% as shown in the table. At 120 kVp the measured HVL was 6.29 mm Al and the calculated HVL was 6.31 mm Al.

kVp	mR Predicted	mR Measured	% Difference
80	329	320	2.76%
100	571	544	4.75%
120	861	808	6.10%
140	1190	1103	7.31%

Table 7 – Comparison of measure and computed (SPEKTR) output for a clinical CT

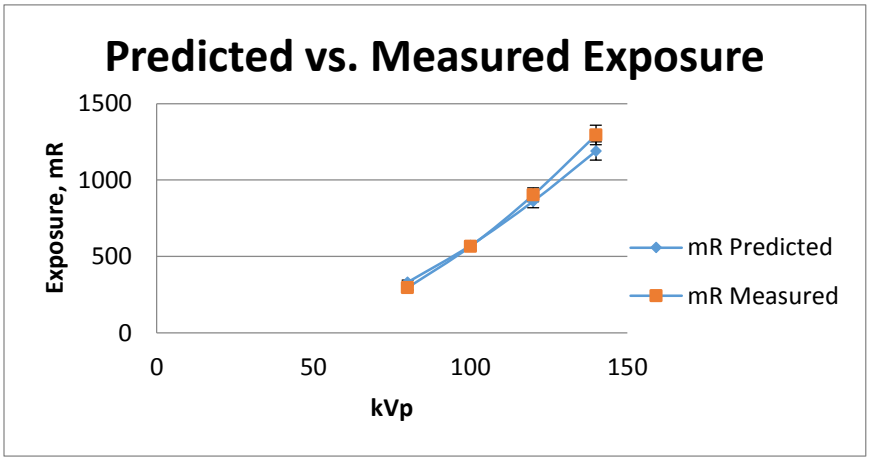

Figure 12 – Graphic comparison of measured and computed (SPEKTR) output for a clinical CT.

All output measurements generated are in air and do not account for scatter. Additional predictions (SPEKTR based) and measurements were made through 8 cm of water and take into

account scatter. A polynomial fit of the scatter correction factor as a function of kVp yields excellent predictability as shown in Table 8 and graphically in figure 10. The scatter to primary ratio is approximately 1.0, ranging from 1.2 at 80 kVp to 0.91 at 140 kVp.

kVp	mR Predicted	mR Measured	Difference
80	295	297	-0.7%
100	565	574	-1.6%
120	902	913	-1.2%
140	1295	1326	-2.3%

Table 8 – Comparison of measured and calculated (SPEKTR) exposure with 8cm of water.

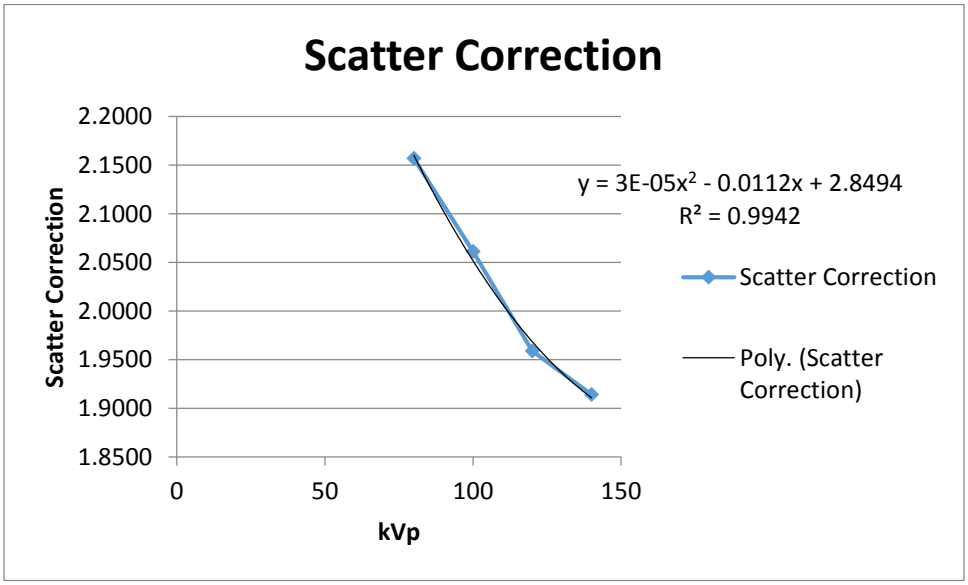

Figure 13 – Graphic comparison of measured and calculated (SPEKTR) exposure with 8 cm water.

3.1.3 Solid water phantom evaluation

The solid water phantom was scanned on a General Electric Lightspeed 16™ CT scanner. Scans were performed at 80, 100, 120 and 140 kVp. The CT number of the phantom was measured near the center of the phantom (while avoiding the centrally located rod) using the workstation provided on the scanner. Scans of the GE supplied water phantom that is used for daily QC were performed using the same parameters.

The CT number of the phantom ranged from 3.44 at 140 kVp to 4.36 at 80 kVp. For the GE QC phantom the range was from -1.55 to -2.92, respectively. The difference between the CIRS phantom and the GE phantom ranged from 4.99 HU at 140 kVp to 7.28 HU at 80 kVp. For this unit General Electric specifies the acceptable range of CT numbers to be -3 to +3 H.U. at 120 kVp. The American College of Radiology (ACR) in their Accreditation manual requires the range to be between -7 and+7 H.U. using the ACR QC phantom which is also fabricated using a solid, water-equivalent, material. From experience it is noted that day-to-day variations of 1 or 2 H.U. in the CT number of the water phantom during routine QC are not uncommon. The agreement between the solid water phantom and the GE QC phantom are acceptable given these observations.

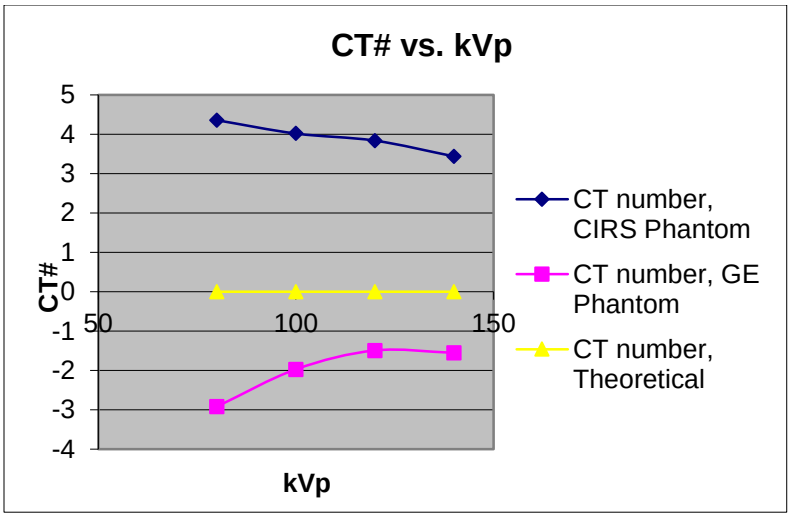

Fig 14 – CT number as a funtion of kVp for the CIRS solid water phantom

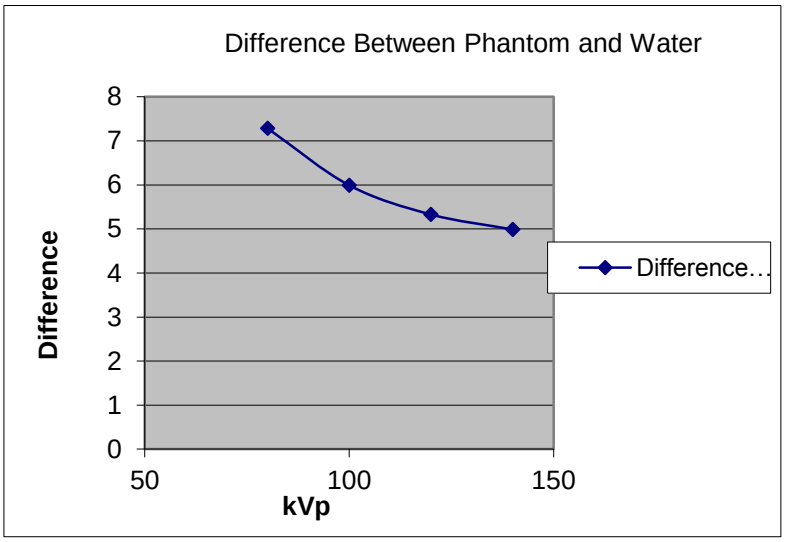

Fig 15 – Plot of the CT number difference between the CIRS solid water phantom and water

3.1.4 Generated Image Data

Using a first- principles computed x-ray spectra at 120 kVp and 8 mm Al filtration, projection data through a 16 cm head CTDI acrylic phantom was computed. The projection data, in photons per square centimeter per 100 mAs, were converted to linear attenuation coefficients for each projected ray. 360 separate projections, each one with Poisson counting statistics applied were acquired. Filtered back projection was applied to the 360 noisy projection data sets to produce a simulated image. This data, in turn, was converted into a DICOM image set. The resulting image is shown in figure 13.

The effective energy of the beam was calculated to be 60 keV. At this energy the mass attenuation coefficients of water and Lucite are 0.206 and 0.193 cm^2/gm, respectively[16]. The density of water is 1.00 gm/cm^3 and for Lucite it is 1.17 gm/cm^3 [16]. This results in the linear attenuation coefficients of water and Lucite to be 0.206 and 0.226 cm^{-1} respectively.

Image noise was made by assuming a Poisson distribution of 360 values of the center detector. A random number generator was used to vary the number of photons reaching the detector using the square root of the number of calculated photons as the standard deviation and applying a random number between 0 and 1 to obtain the number of standard deviations to add or subtract from the number of photons at the detector and then calculating the resulting standard deviation of the calculated linear attenuation coefficients in the center of the model. This resulted in a noise value of 0.28% which is compared to a measured value of 0.39%. Agreement is only fair, at best.

The radiation dose to the center of the simulated phantom was calculated. Figure 16 shows the geometry that was used. The path length to the center of the phantom is 8 cm so the data from ray 94 (8.03 cm path length) was used. The intensity of this ray is 2.15E09 keV/cm^2-mAs

which, when corrected for distance, yields a dose to the center of the phantom of 2.44 mGy/100mAs. This is compared to recent measurements which yielded 2.05 mGy/100mAs. The agreement is within 20%, which is also only fair. Based upon personal experience with CT units, measured dose when compared with doses computed by the manufacturer are usually within 10% of each other. While spectra generated from first principles provided fair results, alternate methods (SPEKTR) to generate x-ray spectra were considered in an attempt to improve accuracy.

This experiment was not repeated using SPEKTR. SPEKTR generated spectra were used to predict the exposure at 80, 100, 120 and 140 kVp in a water-equivalent phantom and the predicted exposures were compared to measured results. This is detailed in section 3.6.

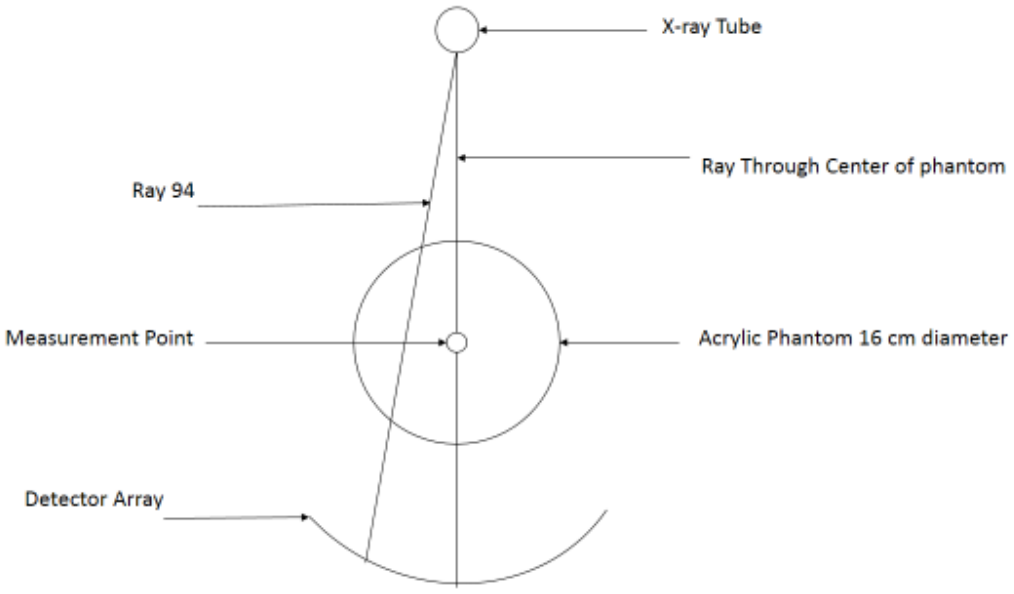

Figure 16 – Geometry for Calculating Dose

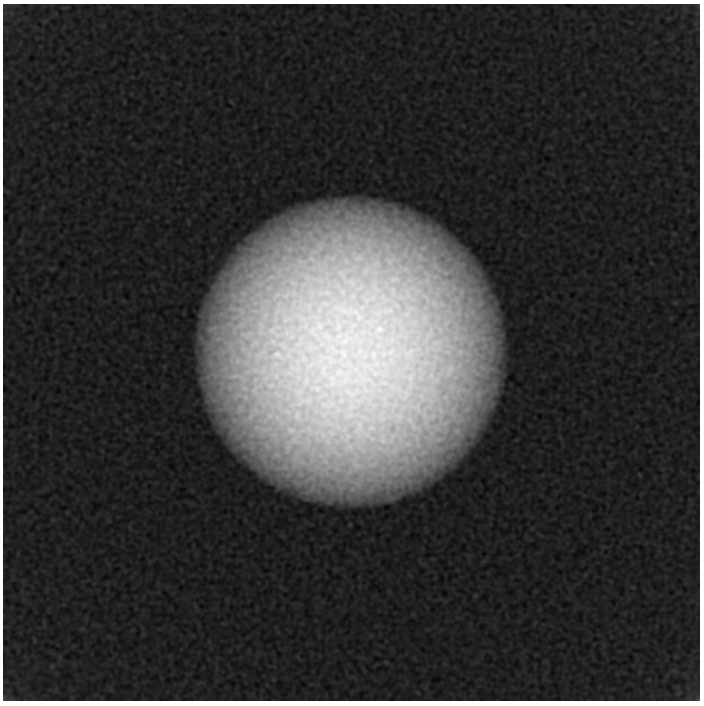

Figure 17 – Generated CT image of a 16 cm acrylic CTDI phantom at 140 kVp and 100 mAs.

3.2 Measured Radiation Dose in Computed Tomography[43]

In the Comparison of MDCT Radiation Dose: A Phantom Study[43], all 60 thermoluminescent dosimeters used for this study are included in the data set and none of the thermoluminescent dosimeters were felt to be far outside an acceptable range. There was a single thermoluminescent dosimeter in the center of the 8-MDCT arrangement that was higher than any of the other thermoluminescent dosimeters. Exclusion of this thermoluminescent dosimeter did not change the data appreciably, although there was an increase in the Standard Deviation in this series.

There was no statistically significant difference by Student's *t* test in radiation dose when comparing the three different scanners using standard departmental protocols, p = 0.06-0.4 (Figure 18). However, a trend of decreasing radiation dose with increasing number of detectors was observed (Figure 19).[43] Further, there was no statistically significant difference observed in radiation dose between the center, anterior, and lateral thermoluminescent dosimeters on or in the Rando phantom when using standard departmental protocols or with a near-identical technique, p = 0.09-0.4 by Student's *t* test (figures 14 and 16).

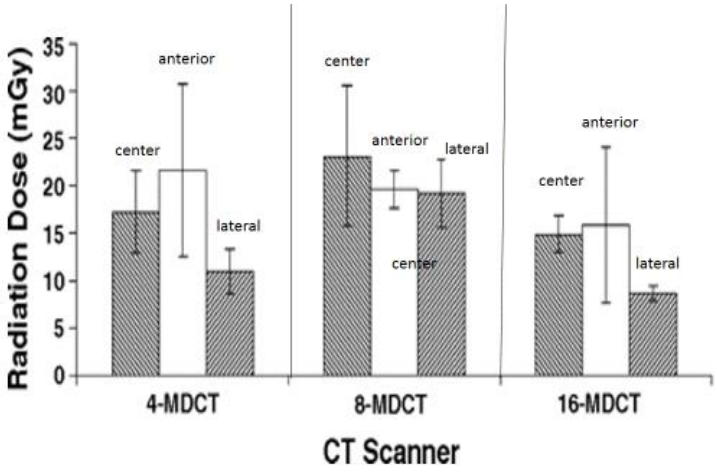

Figure 18 - Radiation dose for 4-, 8-, and 16-MDCT units using standard departmental protocol for CT of chest. Bars represent average radiation dose of five thermoluminescent dosimeters used at center, anterior, and lateral positions, respectively, in slice 18 (midportion of heart) of Rando phantom (The Phantom Laboratory). Error bars are 2 x SD to represent a confidence interval of 95%. (From previously co-authored publishcation[43]). The error bars represent the wide variation in readings that were

obtained with TLD's. There are two main types of error that can occur when performing experiments: systematic and random. Systematic errors refer to those that are inherent in the instrument used to make measurements (such a zero offset or a miscalibration) or in the way in which measurements are made (such as using the wrong setting on a TLD reader). Random errors are those that occur when repeated measurements of the same thing give different results. With the TLD's we found that even though they were exposed simultaneously and read using the same instrument with the same settings the results varied. This could very well be due to a variation in the TLD's themselves. This was suspected because of my personal experience with TLD'

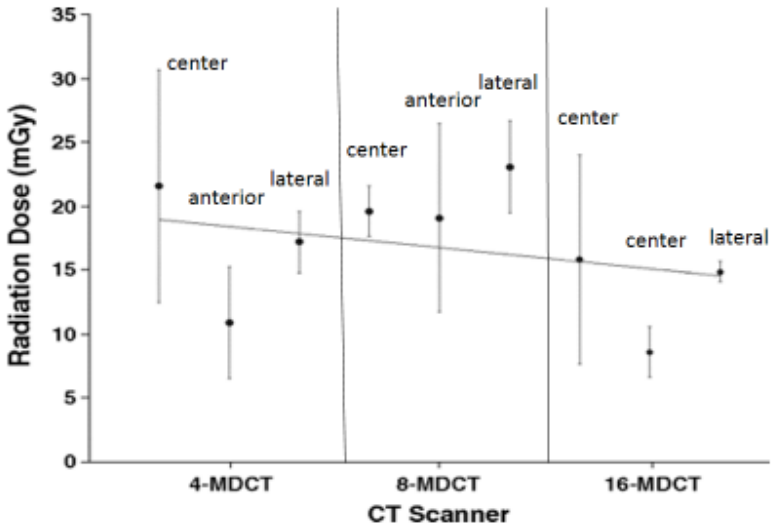

Figure 19 - Trend of radiation dose with standard departmental protocol for 4-, 8-, and 16-MDCT units. Radiation dose is recorded in mGy. Error bars are 2 x SD. Each data point is

average of five thermoluminescent dosimeters placed in center, anterior, and lateral aspects of Rando™ phantom (The Phantom Laboratory).[43]

When the CT units were all set to the same peak kilovoltage, noise, and collimation, there was approximately a 47% higher radiation dose observed with the 4-detector unit compared with the 16-detector unit (figure 16)[43]. This difference is statistically significant by Student's *t* test ($p < 0.01$). A similar statistical difference was observed between the 4- and the 8-detector systems ($p < 0.01$). However, no statistically significant difference was observed between the 8- and the 16-detector units ($p = 0.26$). As with standard departmental protocols, there is a trend toward decreasing radiation dose with an increasing number of detectors (figure 20).

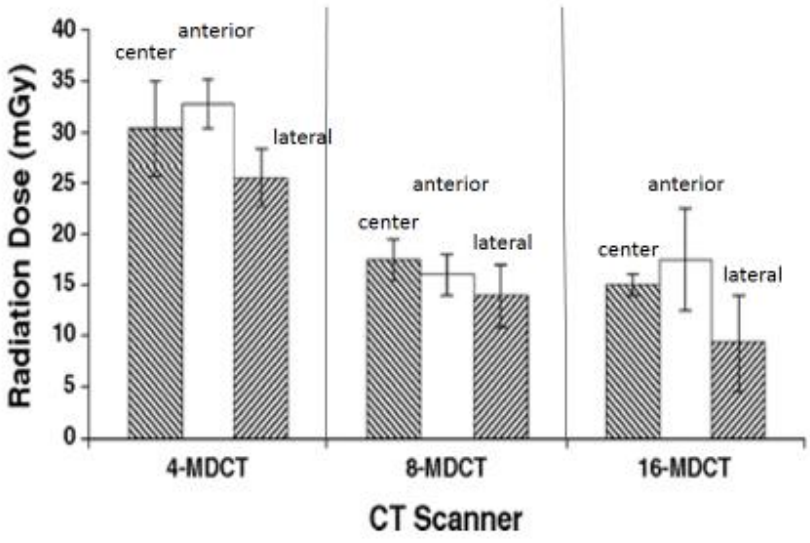

Figure 20 - Radiation dose for 4-, 8-, and 16-MDCT units using near-identical protocols. Bars represent average of five thermoluminescent dosimeters at each site with error bars representing 2 x SD.[43]

We observed a 55% increase in radiation dose comparing the standard departmental protocol to the near-identical protocol on the 4-MDCT unit. This difference was statically significant ($p < 0.01$). There was no significant difference in radiation dose between the 8- or 16-detector units when comparing standard departmental protocol to a near-identical technique[43] (parameters that were set as close as possible to each other for each unit taking into consideration the different capabilities of the 4, 8 and 16-slice units).

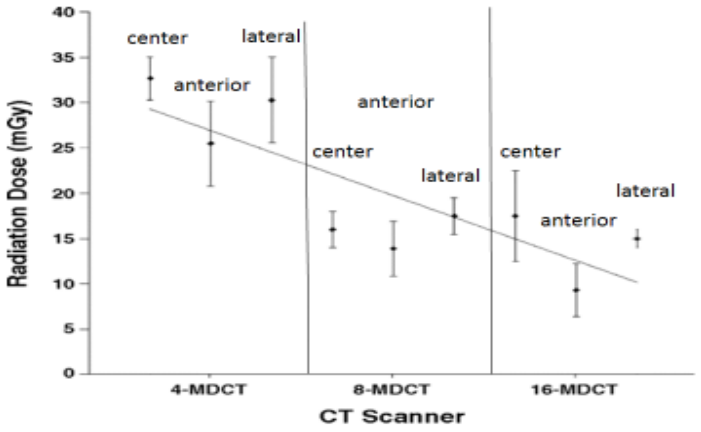

Figure 21 - Trend of radiation dose with near-identical technique for 4-, 8-, and 16-MDCT units. Radiation dose is recorded in mGy; error bars are 2 x SD. Each data point is average of five thermoluminescent dosimeters placed in center, anterior, and lateral aspects of Rando™ phantom (The Phantom Laboratory) [43].

When comparing the measured radiation dose in the Rando™ phantom from the thermoluminescent dosimeter data to the calculated dose-length product (DLP) and effective dose (ED), we found that the measured radiation dose was higher for all the CT units. The calculated dose was underestimated by 1-30%. This correlates with the Groves et al.[58] data,

which showed that the calculated radiation dose was approximately 18% lower than the measured radiation exposure. The trends observed from the thermoluminescent dosimeter data

are echoed by the DLP and ED calculations. We see that there is an increased amount of radiation dose seen with the 4-detector unit when compared with both the 8- and 16-detector units when near-identical technique was used. Also, with standard departmental protocols, there is only a small degree of difference between the radiation doses with all three CT units.

3.3 Evaluation of Contrast Agents in Phantoms[59]

The following is excerpted from a paper co-authored with W. Moore, T. Button, H Weismann, R. Yakupov, and A. Dilmanian[59]. Fig 22 shows the CT image contrast in Hounsfield unites (HU) of iodine and gadolinium as a function of the molar concentrations of the two elements at 120 kVp. The results indicate an about fourfold advantage for Gd. Additionally, the results confirm previous findings[31] of a linear relationship between concentration and attenuation (HU) in both Gd and iodine, **especially at higher concentrations where the effect of the 3× normal saline vanishes** (Emphasis mine). This Gd advantage was statistically significant (P = .01 at concentrations higher than 50 mmole) where the Gd-to-iodine contrast-to-noise ratio (CNR) reached about 5:1.

It should be noted that the clinically accepted limit for human use for gadolinium is 0.6 ml/kg of 0.5 M Magnevist (gadopentetate dimegulmine)[59]. For a 70 kg adult this is 21 mM. For Ultravist (ioprmide) 120 ml of 2.39 M solution is the clinically recommended dose for an adult (for a single injection)[59]. This results in 287 mM for a 70 kg adult.

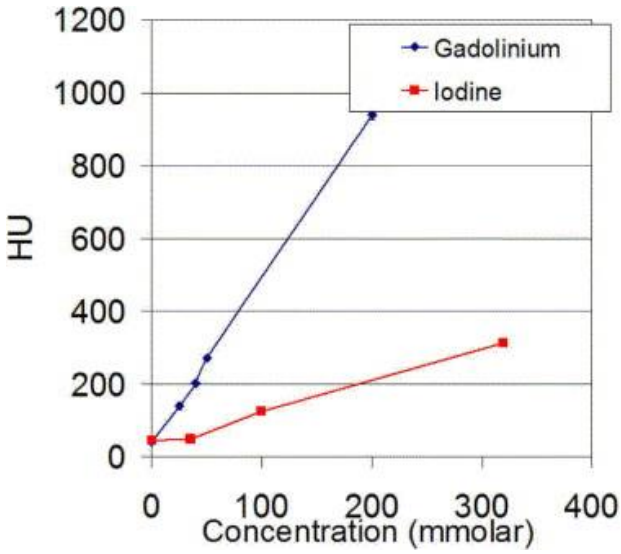

Figure 22 - Computed tomography attenuation, in Hounsfield units (HU) for different concentrations of gadolinium and iodine in a 32-cm acrylic body phantom. All images were obtained at 120 kVp and 300 mAs with a rotation speed of 0.6 seconds. Diamond = gadolinium; square = iodine. Error bars, which are present at all points, are 2× standard deviation[59].

Figure 23 shows the same CT image contrast as in figure 22 except as a function of kVp for the 50 mmole concentration of the two elements. The results indicate an inverse relationship between kVp and attenuation. An average of 24% increase in the attenuation of the CT beam is observed when comparing 80 kVp to 120 kVp[59].

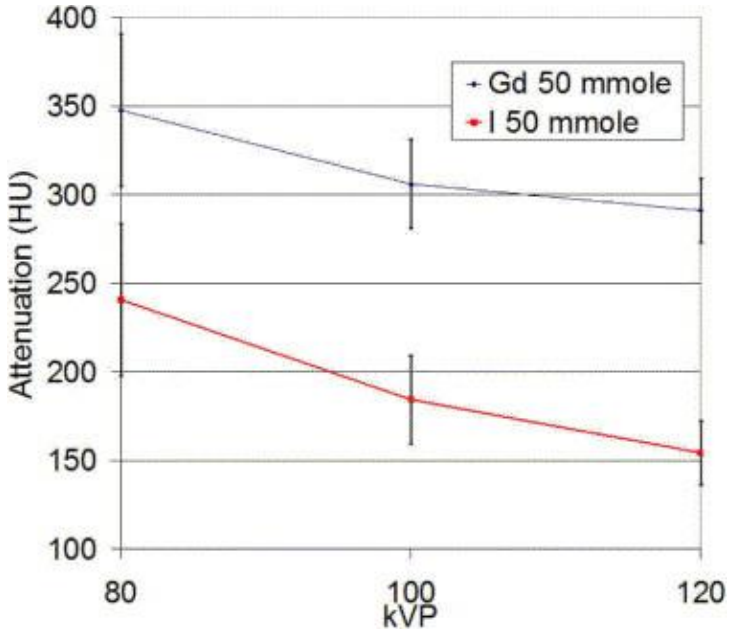

Figure 23 - Computed tomography attenuation (Hounsfield units) for 50 mmole gadolinium and iodine at 80, 100, and 120 kVp, all images were obtained at 300 mAs. Diamond = 50 mmole gadolinium; square = 50 mmole iodine. Error bars represent 2× standard deviation[59]

3.4 Evaluation of Contrast Agents in Animals[59]

This experiment was performed using the General Electric Lightspeed 16-slice unit that has been used previously. The 80 kVp spectrum is the standard spectrum (unaltered) from the x-ray tube of this unit. The spectra that were used in the model is based upon this x-ray tube.

All measurements were taken at the arch of the rabbit's aorta at approximately 10 seconds and 5 and 10 minutes after the completion of the contrast agent's injection. Figure 24 shows the attenuation (HU) over time, comparing injection volumes of 20 mL of Gadovist™ and Ultravist™ with 6 mL of Magnevist™. The total time to complete the injection is estimated to be 15 seconds for Gadovist™ and Ultravist™ and less than 5 seconds for the Magnevist™

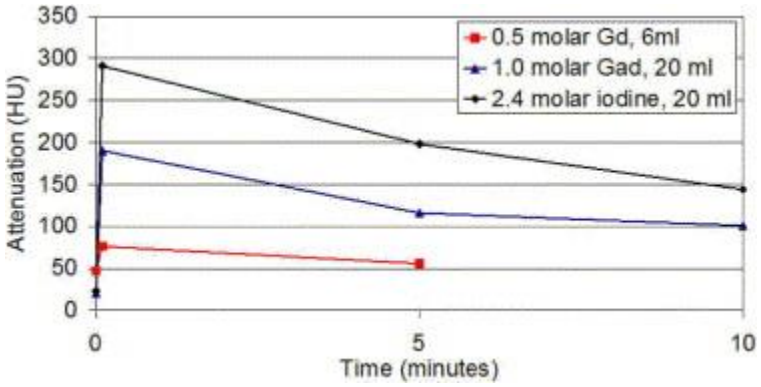

Figure 24 - Change in computed tomography contrast at 80 kVp of the rabbit's aortic arch in three time points after the administration of two Gd-based contrast media and one iodinated (6 mL of 0.5 molar [Magnevist™], 20 mL of 1.0 molar [Gadovist™], and 20 mL of 2.4 molar iodine [Ultravist™]) contrast media. The first image was obtained at 10 seconds after the injection of contrast. Diamond = 2.4 molar iodine; square = 0.5 molar, 6 mL of gadolinium; triangle = 20 mL of 1.0 molar gadolinium[59]

The results show about a 2.5-fold larger attenuation (HU) for Gadovist™ versus Magnevist™, and a 1.5-fold larger attenuation for Ultravist™ versus Gadovist™. The latter can be explained by a 2.4-fold larger molar concentration of the contrast elements in Ultravist™ and about a 1.5 times larger attenuation of Gd versus iodine for the same molar concentration as measured in our phantom studies. However, a third and fourth factors, namely the physiologic ones involved in these two studies including the different injection rates and different dilutions in the rabbit's body, are difficult to estimate. In particular, the dilution factor could have been affected by slight difference in the injection rates we had in the two compounds and by the difference in their viscosities and other physical properties. As for the injection rates, the time it took to inject the volumes of contrast media was much longer in the 20-mL studies with

Ultravist™ and Gadovist™, approximately 15 seconds, compared with the 6-mL Magnevist™ study, which took approximately 5 seconds.

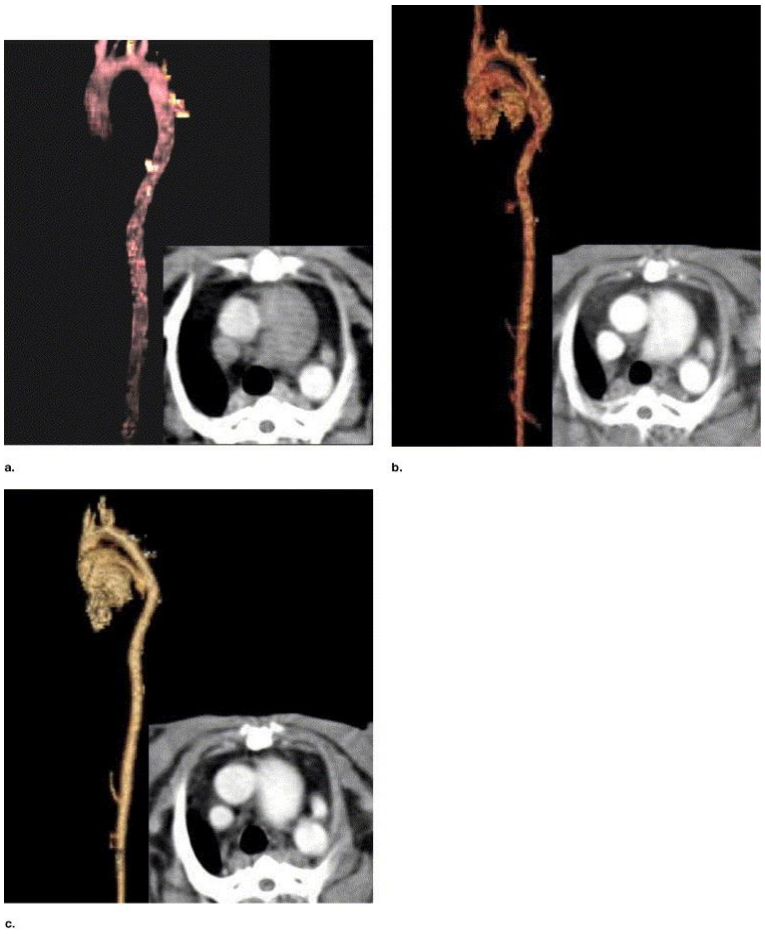

Figure 25 - Three-dimensional (3D) volume rendered reconstructed images with inlayed axial images in soft-tissue windows of the rabbit aorta.

All images were started at approximately 10 seconds after the injection of contrast and all images were obtained at 80 kVp. **(a)** 3D reconstructed image with inlayed axial image with 5 mL of 0.5 molar gadolinium agent (Magnevist™); **(b)** 3D reconstructed image with inlayed image

with 20 mL of 2.4 molar iodine agent (Ultravist™); **(c)** 3D reconstructed image with inlayed image with 20 mL of 1.0 molar gadolinium contrast (Gadovist™)[59].

Qualitative enhancement of the aorta was observed with both Gd solutions at all three kVps. Quantitatively, for the set of data obtained with the shortest elapsed time, the CNR observed in the rabbit aorta at our highest kVp (120 kVp) was still about 15:1, which far exceeds the minimum 5:1 detectable CNR suggested by Rose[77]. Figure 14 a,b,c show three-dimensional volume renderings of the rabbit aorta with Magnevist™, Ultravist™, and Gadovist™, respectively.

For the 5-minute elapsed time, the attenuation of the rabbit aorta was still visible for all agents and for all kVps except for the 120 kVp with Magnevist™ (figure 26). For each of the contrast media, there was greater attenuation at the lowest kVp, which is similar to the effect observed in our phantom studies.

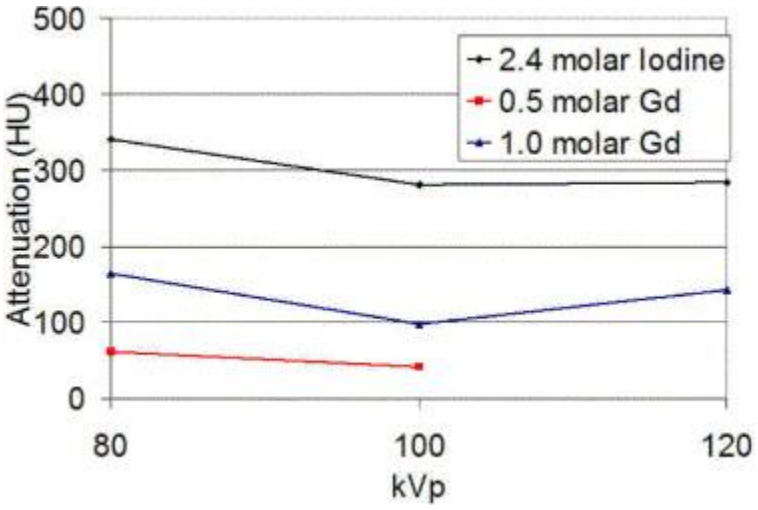

Figure 26 - Computed tomography attenuation (Hounsfield units) of the rabbit aortic arch 5 minutes after injection of the three different contrast media with varying kVp values. Diamond = iodine; square = 1.0 molar gadolinium; triangle = 1.0 molar gadolinium[59].

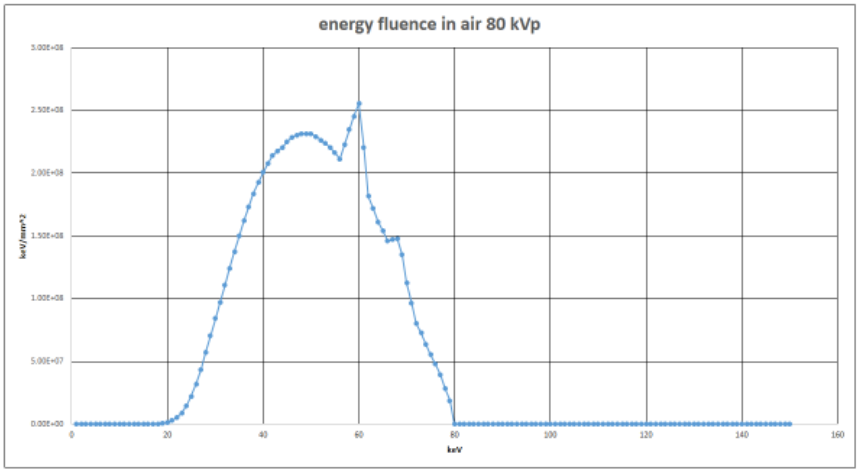

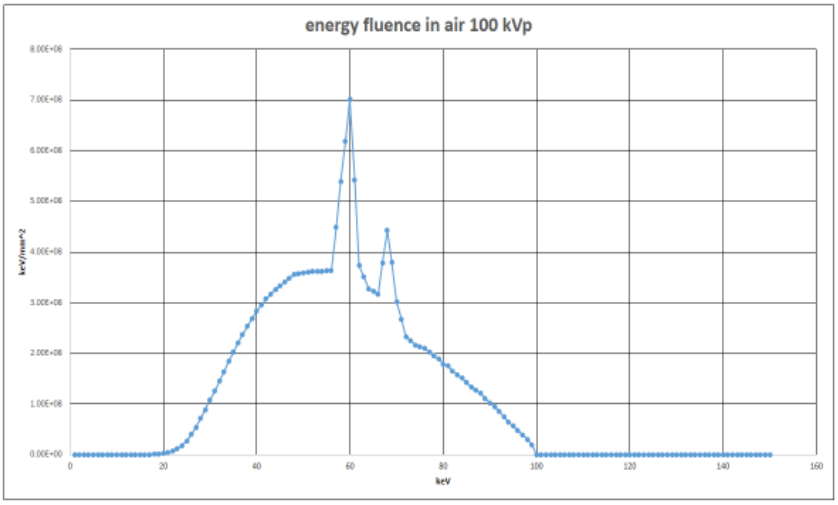

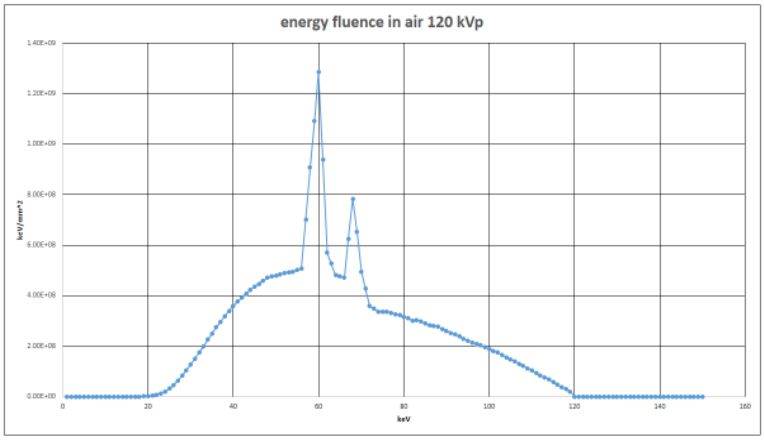

Figure 27 – Energy Fluence Spectra at 80, 100, and 120 kVp with 5.0 mm Al + 2*u*m W filtration

3.5 Comparison of Iodine and Gadolinium using the Contrast Agent Evaluation Model

At 120 kVp the measured CT numbers of gadolinium concentrations of 0.5, 5 and 50 mM in the test phantom were 3.6, 27 and 282 respectively. The calculated CT numbers derived from the 120 kVp spectrum with standard filtration (5.0 mm total Al plus 2*u*m W added) generated by SPEKTR for the same concentrations of gadolinium are: 3.0, 30, and 296, respectively. This

spectrum was found to yield measurable results that well matched the output of the x-ray tube on this unit (output in mR/mAs and HVL at 120 kVp). Energy fluence at the detectors is utilized for these calculations. A plot (Figure 28) compares these two results.

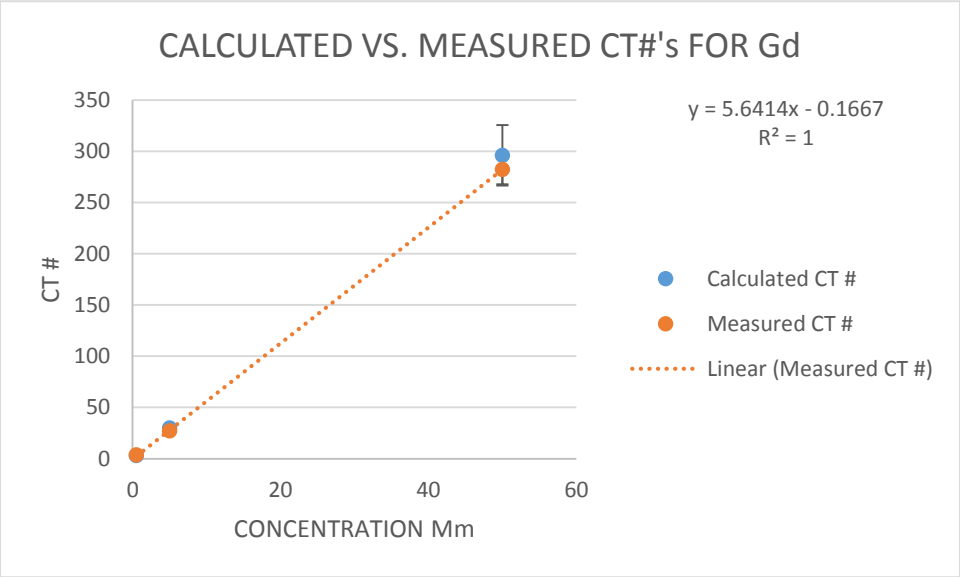

Figure 28 Predicted vs. Measured CT numbers of Various Concentrations of Gadolinium

3.6 Radiation Dose

The ability of SPEKTR to accurately predict the exposure rate in air and the HVL at kVp's ranging from 80 to 140 has been demonstrated. Once the attenuation of the water phantom is introduced, however, SPEKTR grossly underestimates the exposure. This is due to the inability of SPEKTR to account for scatter. It was necessary to develop an empirical correction for scatter.

As previously described, measurements of the exposure in the center of the water phantom were made at 80, 100, 120, and 140 kVp. The measurements were made using the same General Electric Lightspeed Ultra CT scanner that was described previously. The collimation along the z-axis was set to 20 mm (the maximum available on this unit) and a 0.6 cc chamber (Radcal 10X5-0.6) was placed in the center of the phantom.

Figure 29 shows the relationship between measured and calculated (from SPEKTR with 8 cm water attenuation) exposures in the center of the water phantom at 80, 100, 120 and 140 kVp. Clearly the calculated demonstrates reduced exposure because scatter has not been taken into account.

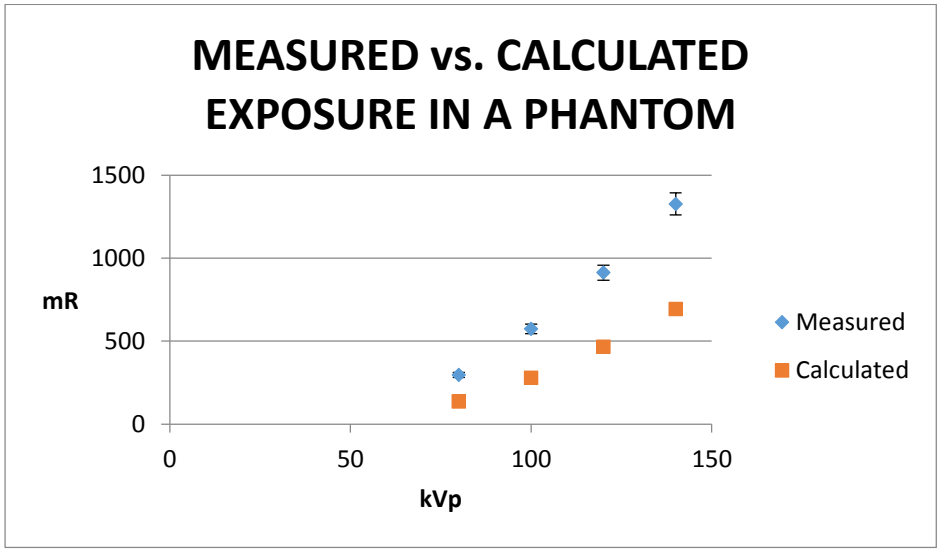

Figure 29 – Measured vs. Calculated Exposure in a Phantom

The resulting correction factor as a function of kVp are provided in Table 9 and Figure 25. All radiation exposures and doses provided from SPEKTR generated spectra will, therefore, be scatter corrected by these empirically determined corrections. Dose was calculated by using an f-factor of 0.0009 rad/mR (0.009 mGy/mR).

80 kVp	2.16
100 kVp	2.06
120 kVp	1.94
140 kVp	1.91

Table 9 – Correction factors used to compensate for scatter

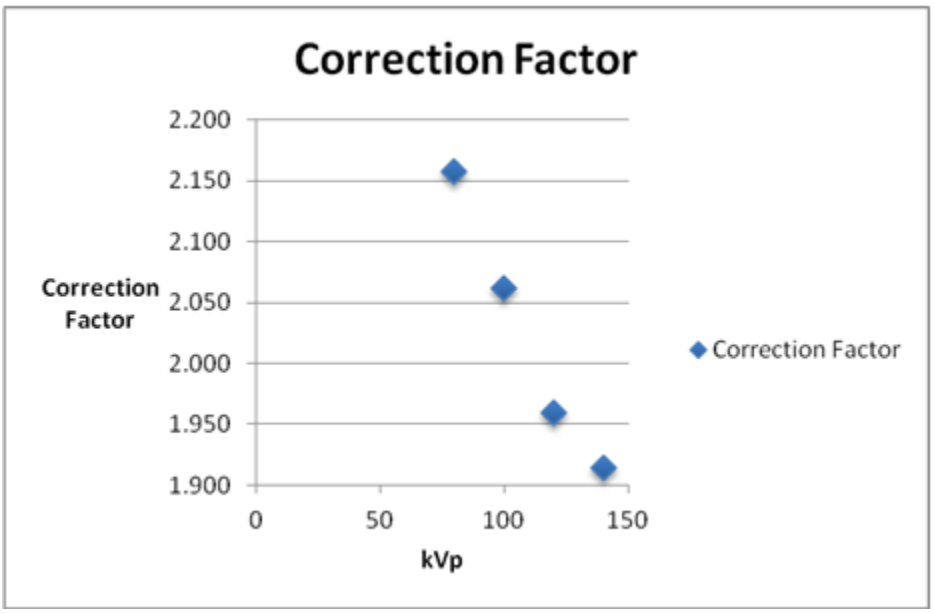

Figure 30 – Correction factors used to compensate for scatter.

3.7 Evaluation of Iodine and Gadolinium using the Contrast Agent Evaluation Model

Results above demonstrate that SPEKTR generated spectra can be used to accurately predict air exposure, dose (with scatter corrections), HVL, and CT numbers. These spectra could also be employed to compute projection data and a predicted image appearance. As described, however, the details of image generation have a variety of problems that make it difficult to access CNR for a contrast target containing phantom. First, although Matlab™ is capable of producing filtered backprojection images, there are difficulties. These include: a grey scale that is limited to 8 bits instead of the minimum of 11 needed to reproduce the full range of CT numbers, difficulty in converting the .jpeg images to DICOM images, and scaling the DICOM images to at least 11 bits. The selection of a reconstruction filter that replicated the reconstruction filter utilized by the clinical unit (so that meaningful comparisons could be made) was not possible. To avoid these difficulties I instead employed only the projection data (with noise) without actually generating an image. The CNR_i in an image acquisition was simply determined from the projection data CNR_p by correcting for propagation of error or other errors. This correction was done empirically as described previously.

An empirical correction for noise propagation was determined using Gadolinium based contrast agent. Projection data was computed for a GE lightspeed CT at 120 kV (with 5.0 mm Al and 2 *u*m W filtration) and 350 mAs for a 0.5, 5 and 50 mM gadolinium filled targets in the solid water phantom by calculating the energy fluence through the contrast filled vial in the phantom and using the absorption through the contrast filled vial compared to the absorption through water the contrast was determined. The noise was calculated by using the square root of

the intensity for each detector as the standard deviation, applying a random number that varies between 0 and 1 as the probability for the normal distribution function and then calculating the expected signal at the detector which is the mean intensity with the square root added or subtracted depending upon the value of the random number that was generated. The standard deviation of 20 iterations of calculating the mean of the detectors immediately surrounding the contrast-filled section was calculated. The standard deviation is then the noise. The CNRp is the CT number of the contrast-filled section divided by the calculated noise.

The projection data for 0.5 mM is shown in figure 26. In this case the projection data $CNR_p = 51.4$.

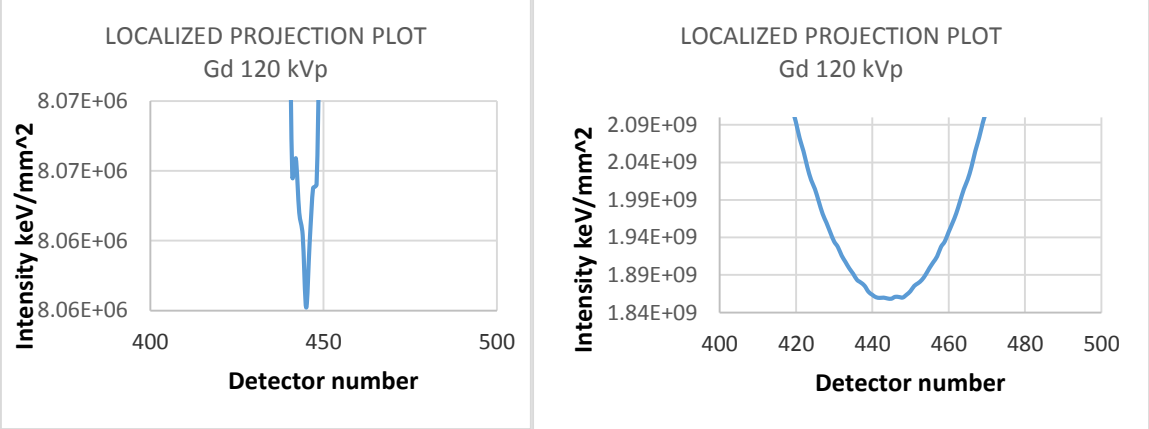

Figure 31 – GE Lightspeed at 120 kV and 350 mAs calculated projection data through the solid water phantom with a 0.5 mM gadolinium target

Similar calculations were done at 5 and 50 mM as well. In addition, 0.5, 5 and 50 mM target solutions were placed in the solid water phantom and GE Lightspeed CT image data acquired at 120 kV and 350 mAs. Regions of interest (ROIs) in the target and in a water filled

vial in the same position as the target were used to determine CNR in the image at each concentration as shown in figure 27. A water filled vial was used instead of the region of the phantom next to the contrast filled vial because the net difference between water and contrast is what is of interest. The calibration of this unit is such that water usually has a CT number somewhat less than zero.

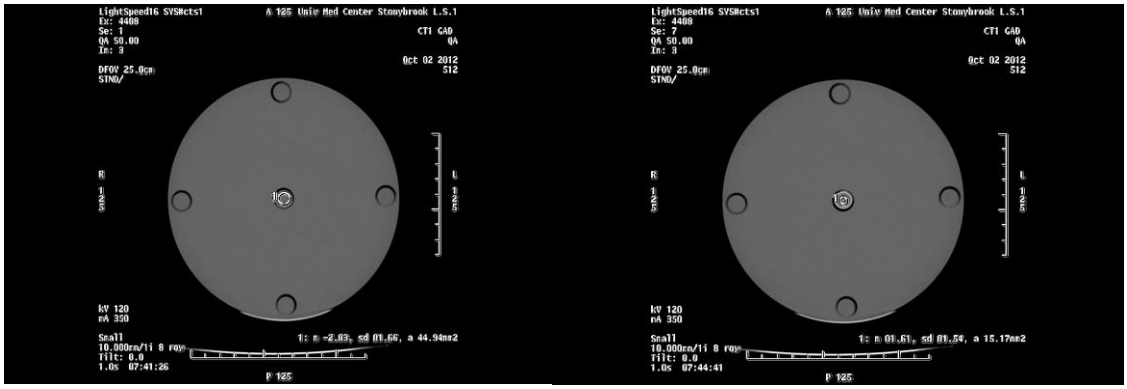

Figure 32 – Water Filled Vial on the Left and 0.5 Mm Gd on the Right Showing CT numbers and Standard Deviation

For the model the contrast-filled vial is in the center of the water phantom. The phantom is at the isocenter (54 cm from the focal spot) of the CT unit. The center ray (at detector 444) is used to determine the attenuation due to the contrast media solutions. The surrounding rays (440 and 450) which do not contain contrast are used to calculate noise.

These calculations resulted in the following projection CNR and image CNR estimates for gadolinium:

Gd concentraton	projection CNR	image CNR	correction
5.0 mmol	541.00	16.60	32.6
50 mmol	5103	170.0	30.0

Table 10 – Determination of propagation of error correction

Based on the data above, the propagation of error correction is approximately 31.3 (the mean of the two concentrations tested). The empirical correction factor for propagation of error was confirmed in the case of iodine as well. Sample calculated projection data from a GE Lightspeed CT at 120 kV and 260 mAs for a 2.92 mM iodine filled target in the solid water phantom was used In this case the projection data CNR = 132.93. Applying correction (132.93/31.3) yields 4.25 while the image CNR measured was 4.29. Agreement is reasonable. The 0.93% discrepancy is acceptable. It was felt that a large difference that was seen at 0.5 mM was attributable to errors made in mixing the very dilute solution. For this reason this data point was not used.

As previously described, in CT, the resolution of objects whose attenuation is close to the attenuation of the surrounding tissue depends upon: the difference in attenuation (contrast), the variation in calculated attenuation (statistical noise), and the size of the object. For the purpose of evaluation of contrast agents, it is important to determine the minimum concentration that will render iso-intense anatomy detectable per unit radiation dose. The selection of contrast-to-noise

value required for detection is arbitrary. The American College of Radiology CT phantom has low contrast structures which are scored for detection based on a contrast-to-noise ratio (CNR) of approximately 1[81]. This seems a reasonable base line. Therefore, for this work we will determine contrast agent concentration required for detection with a CNR of 1.

3.8 Application of the Contrast Agent Evaluation Model

Components required for the contrast agent evaluation model worked quite well. Using an empirical factor to account for propagation of error, CNR_i could be accurately computed from SPEKTR generated spectra for a variety of contrast agent containing targets. Similarly, by correcting for scatter, dose delivered could be accurately predicted using SPEKTR generated spectra. Based on these results, we applied the contrast agent evaluation model to a variety of kV and filter combinations for both iodine and gadolinium contrast agents. The spectra containing 50 *u*m of tungsten filtration are experimental; these were not imaged. The calculated minimum effective concentration for several of these are shown in table 11 below.

What is interesting to note is that for all of the conditions studied gadolinium appears to be a more effective contrast agent than iodine. A lower MEC appears to be needed to obtain the same CNR. This would also imply that, for an equivalent CNR, a lower radiation dose could be used if gadolinium was substituted for iodine. This also implies that 80 kVp, even with standard filtration, should be considered when iodine is used as a contrast medium. Table 11 shows the calculated MEC's based upon the model.

Condition	minimum effective concentration
I at 120 kV	0..74 mM
I at 80 kVp	0.49 mM
I at 80 kV with 50*u*m W filter	0.64 mM
Gd at 120 kV	0.50 mM
Gd at 80 kV with 50μm W filter	0.44 mM

Table 11 – Minimum Effective Contrast Agent Concentration

Two spectra are shown below; the first is 80 kVp with 5.0 mm Al and 2*u*m W with 50 *u*m of added W to put the majority of the intensity above the k-edge of gadolinium and the second is 80 kVp without the added tungsten (standard filtration). While both spectra are attenuated by both gadolinium and iodine the spectrum with added tungsten does have more of its intensity above the k-edge of gadolinium than the spectrum without added tungsten. Both spectra peak above the k-edge for iodine.

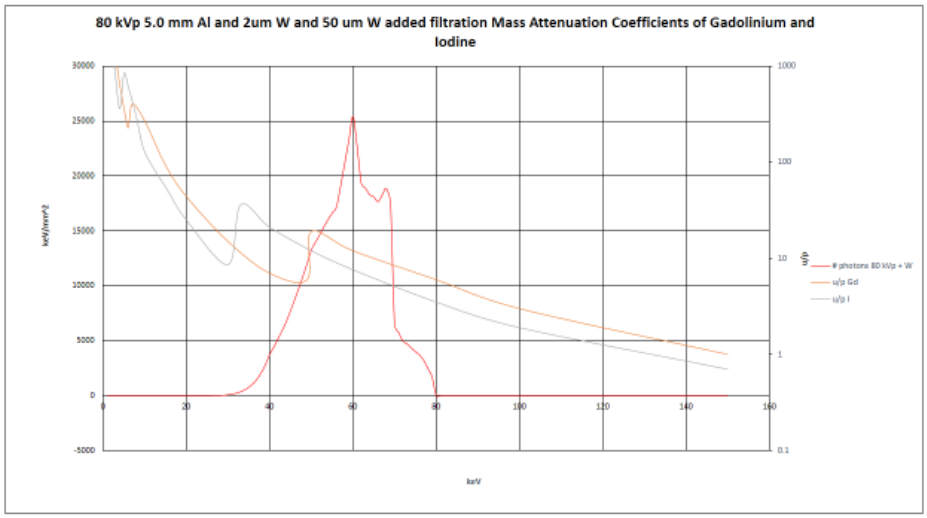

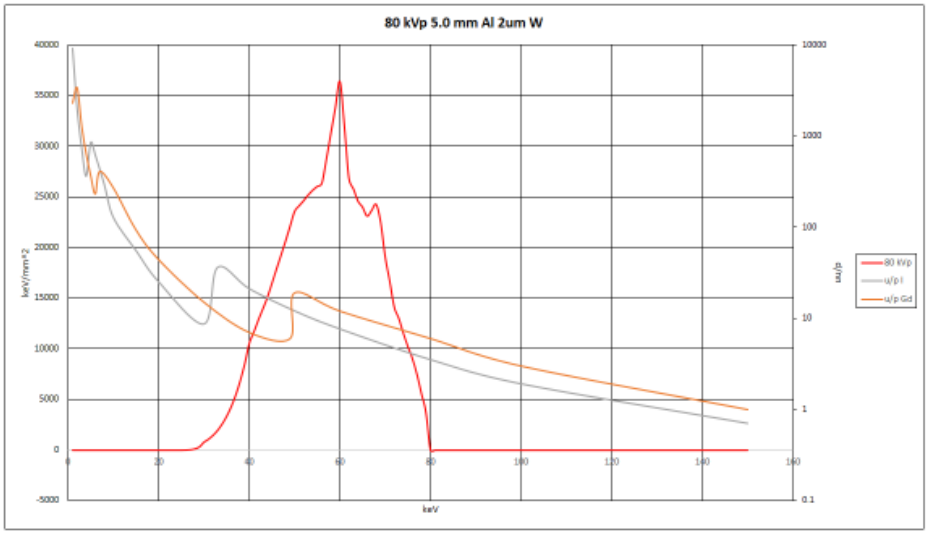

Figure 33 – 80 kVp spectra through the phantom with and without added W filtration

One limitation of this study is that calculating MEC involved calculating the CNR from CNR_p by using an empirically derived factor from CNR_i at a single kVp. A better approach would be to look at noise as a function of kVp. One could conceivably use physical models that are available to determine noise as a function of kVp and dose. CT numbers should track lineally with concentration. Once this is done testing the performance of new spectra would involve determining the dose to the phantom (to determine noise) and calculating the CT number of the contrast material of interest with the new spectrum. This would not involve the complicated procedure of calculating CNR_p and the correction factors that have been described.

4. Discussion

4.1 Contrast Agent Evaluation Model

Overall, the spectrum calculated from first principles agrees well with that measured by Birch. There is a 2% difference in the total number of photons across the energy range. At low energies the calculated spectrum is more intense while at higher energies the measured spectrum is more intense. The measured spectrum also contains more characteristic photons than the calculated spectrum.

The increased intensity at low energy could be due to the calculations not accounting for the glass and oil of the x-ray tube assembly. These low energy photons can probably be safely ignored as they would be completely absorbed by the patient (if they were present) and therefore not contribute to the image.

The higher energy photons will, however, contribute most to image formation in CT. It is possible that underestimating the contribution of these photons could underestimate the eventual Signal-to-Noise Ratio in the image. Additionally, the measured parameters of output (mR/mAs) at various kVp's do not agree well with those predicted using first principles. For these reasons SPEKTR-based spectra were considered. The spectra generated by SPEKTR yielded results that accurately predicted both output and HVL over clinically relevant conditions: general radiographic kVp/filter combinations and CT.

Generated image data from the spectra is encouraging. The noise in the calculated image agrees favorably with actual images collected under similar technical factors. There are difficulties, however, that preclude its use: it is only 8-bit, the reconstruction filter does not necessarily match the clinical unit, and corrections that are needed to account for these.

4.2 Radiation dose in Computed Tomography[43]

The following is excerpted from: Comparison of MDCT Radiation Dose: A Phantom Study[43]. When comparing standard technique, there is not a significant difference between any of the detector arrangements (4, 8, and 16-detector row configurations) we tested. However, there is a trend toward decreasing radiation dose with the increasing number of detectors (figure 19). When comparing near-identical techniques, there is a statistically significant decrease in the radiation dose from the 4- to the 8-detector units and the 4- to the 16-detector arrangements. There is a trend toward decreasing radiation dose with the increasing number of detectors figure 21.

When comparing standard technique, the 8-detector unit has a slightly higher radiation dose than the 4-detector unit. Some of the reasons for this finding are related to the unit's configuration. The 4-detector unit is set up to have 4 detectors at 2.5-mm collimation each. There is a nominal pre-patient collimation of 10 mm with an actual pre-patient collimation of 13 mm. The 8-detector unit is set up to have 8 detectors at 1.25 mm each, also with a nominal pre-patient collimation of 10 mm and an actual pre-patient collimation of 13 mm. The pitch used on the 8-detector unit was lower than that used on the 4-detector unit, which can account for the slightly higher radiation dose between these two units. In addition, the noise index for the 4-detector unit

was higher than that of the 8-detector unit, thus resulting in a higher mA being used at slice 18 of the phantom with the 8-detector unit, which further increases the observed radiation dose.

The 16-detector unit is set up with 16 detectors at 1.25-mm collimation each. There is a nominal pre-patient collimation of 20 mm with an actual pre-patient collimation of 21 mm. Therefore, to generate the same CT beam coverage, the 4- and 8-detector units will require 26 mm of exposure compared with 21 mm with the 16-detector unit. This can explain the decreased radiation dose and the observed trend toward decreasing radiation dose with increasing detector configurations. Although this is an accurate portrayal of how these systems function, the actual implementation of this concept is far more complicated because of the helical nature of the image acquisition, which results in overlapping beams of radiation.

When using a near-identical technique, the 4-detector system was less dose-efficient. The reason for this difference could be related to the size of the pre-patient collimation. The 4-detector system has a pre-patient collimator opening of 8.0 mm using 4 detectors at 1.25 mm. The nominal size of the detector array with this configuration is 5 mm, resulting in 3.0 mm of wasted or non-target radiation. We would therefore expect an increase in radiation dose of approximately 66% compared with the 16 x 1.25 mm array. This is close to our observation of an average increased radiation of 47%. The variance of this observation from the calculated result could also be related to several factors: First, the 4 x 1.25 mm configuration had a pitch of 1.5:1, whereas the 16 x 1.25 mm configuration had a pitch of 1.35:1. Second, differences in the noise index and thus the mA used in these images help to account for the differences in the observed radiation dose. Finally, the 16-detector unit is not perfect; there is a 1-mm area of wasted radiation. This additional wasted radiation further accounts for the differences between the calculated and observed radiation dose.

Given these changes in pre-patient collimation, we would calculate an increased radiation dose of 23% when comparing the 4 x 2.5 mm configuration to the 4 x 1.25 mm configuration. This is less than the observed 55% increase in radiation dose. Some of the additional change in radiation could be explained by the increasing number of tails of radiation exposure with the smaller detector configuration. In addition, the noise index that was used for the 4-detector unit was based on the 2.5-mm images. Given that noise decreases with increased slice thickness and that the mA chosen by SMART mA on the 1.25-mm images was higher than on the 2.5-mm images, we would expect higher radiation dose with the 4 x 1.25 mm configuration. The 8-detector unit at 1.25 mm has a pre-patient collimator opening of 13 mm. Thus, this system has 20% less non-target radiation than the 4-detector array at 1.25 mm when covering the same volume. In addition, for the same 20-mm volume of coverage, the 4-detector array will have eight overlapping tails of wasted or non-target radiation, whereas the 8-detector array will have four overlapping tails. Finally, the 16-detector array will only have two overlapping tails. This trend of decreasing overlapping tails of radiation exposure could explain some of the additionally observed decrease in radiation dose with an increasing number of detectors.

This study does have several limitations. First, the use of thermoluminescent dosimeters introduces significant bias. These devices are small and have a tendency to have spurious measurements, requiring exclusion of multiple thermoluminescent dosimeters in most studies. We were able to include all thermoluminescent dosimeters in these data sets.

Second, a standard dose graph was used to estimate the radiation dose obtained from the thermoluminescent dosimeters. This technique can result in mis-calibrations at many levels. However, many studies have used this technique to evaluate radiation dose [47-51]. Although the

most reliable manner to estimate radiation dose is an ionization chamber, this is not a reasonable alternative with phantom work, primarily for physical reasons.

Third, it is not possible to make identical exposures with each of the different CT units. The 4-detector unit only allows two different pitches, 1.5:1 and 0.75:1. These pitches are not available on the 8- and 16-detector units (8- and 16-detector experiments were performed at 1.375:1). We used the 1.5:1 pitch in the 4-detector unit, which could potentially lower the radiation dose seen in the 4-detector unit.

Fourth, slight differences in generator calibration could have resulted in differences in the overall radiation dose. Finally, although there is a trend toward decreasing radiation dose, statistical significance was only shown between the 4-detector unit and the 8-detector unit and between the 4-detector unit and the 16-detector unit. There was no statistically significant difference between the 8- and 16-detector units. Some of these limitations could explain why there was not a statistically significant difference observed with the standard departmental protocol.

Future studies will be needed to evaluate the dose efficiency of new, higher-detector array units, such as the currently available 64-detector unit. If the trend of decreasing radiation dose continues, this may suggest that higher-detector units should be used on a larger scale in an attempt to decrease radiation dose to the public, especially in centers where a large volume of pediatric CT is performed.

4.3 Evaluation of Contrast Agents in a Phantom[59]

The following is excerpted from a paper co-authored with W. Moore, T. Button, H Weismann, R. Yakupov, and A. Dilmanian[59]. Our phantom studies in preparation for animal studies demonstrated a fourfold higher CT image contrast (HU) for Gd compared with iodine for the same molar concentrations of the elements and the same x-ray energy spectrum. They also indicate that lowering the kVp setting from 120 to 80 increases the CT image contrast (HU) for the same molar concentration of both gadolinium and iodine by about 24%.

4.4 Evaluation of Contrast Agents in an Animal Model[59]

The following is excerpted from a paper co-authored with W. Moore, T. Button, H Weismann, R. Yakupov, and A. Dilmanian[59]. Our in vivo model showed that the CT image contrast observed in the rabbit aorta for 2.4 molar iodine (Ultravist) and 1 molar Gd (Gadovist) injected at the same injection volume are qualitatively comparable. They also show that, interpolating the rabbit results to clinically safe volumes of Magnevist (6 mL for a 7-kg rabbit, relating to 60 mL for a 70-kg patient) produces a usable image contrast for CTA; this result makes Magnevist feasible but less well suited alternative to iodine for CTA of the aorta.

Table 12 summarizes the information relating to the doses we used in these studies to the lethal dose in 50% of mice (LD50) and to the clinically practiced doses. The table is meant to produce a common scale for evaluating the relative sizes of the doses given to the rabbit. With regard to the clinically used single dose of Magnevist as indicated in the table, recent studies have assessed the use of 0.4 mmol/kg in humans [78-79]. Most recently, Remy-Jardin prospectively looked at the use of Gd for pulmonary arterial CTA and found that this technique is plausible [80].

Contrast medium	Gram concentration	Lethal dose (LD50)	Volume injected in the rabbit	Dose to the rabbit	Percentage of lethal dose	Clinically used single dose	Ratio of dose to the rabbit to the recommended dose in humans
Ultravist 300 (2.4 mol I/L)	300.0 mg I/mL	153 mmol I/kg: 19.4 g I/kg	20 mL	857 mg I/kg	4.4%	120 mL in a 70-kg human	1.8:1
Gadovist (1.0 mol Gd/L)	157.3 mg Gd/mL	25 mmol Gd/kg; 3.9 g Gd/kg	20 mL	449 mg Gd/kg	11.4%	0.3 mmol/kg	8.9:1
Magnevist (0.5 mol Gd/L)	78.6 mg Gd/mL	6 mmol Gd/kg; 0.9 g Gd/kg	6 mL	67.4 mg Gd/kg	6.0%	0.3 mmol/kg	1.3:1

Table 12 - Comparison of contrast concentration used in this study[59]

The fourfold advantage in the CT image contrast of Gd over iodine in the phantom studies with the same molar concentrations of the elements does not matched the observed results with the rabbit. This effect can be explained as a result of the following factors. Comparing Ultravist™ and Gadovist™, and considering the 2.4:1 molar advantage of Ultravist™, we expect a 1.7-fold higher contrast for Gadovist™. However, the results indicate a 1.5:1 advantage for Ultravist™. This 2.6-fold discrepancy could be explained by the following factor; Gadovist™ is a more viscous material than Ultravist™ therefore, it could have taken a slightly longer time for it to enter the arterial blood stream, resulting in us missing the peak of contrast enhancement of Gadovist™ even at the first kVp tested (ie, 80 kVp). Furthermore, the two other kVp settings (100 and 120) were delayed each by about 6 seconds, which further took us away from the peak enhancement. Additional evidence for this hypothesis can be found in the relatively higher image contrast from Magnevist™, which is a less viscous agent. Although these idiosyncrasies limit the accuracy of our results, they indicate the large number of factors that affect comparative studies of media needed to evaluate their potential for use in clinical CTA.

Putting the results in the context of the potential clinical application of Gadovist™ in clinical CTA, one sees a large gap between the clinically accepted dose and that used in our study. However, this should not exclude the possibility of the use of Gadovist™ because the LD50 results show that the compound is very safe and therefore it is possible that the acceptable dose will be raised in the future, and the clinical usage of Gadovist™ will not require the level of contrast obtained with the full dose of Ultravist™ and therefore there is much latitude to apply Gadovist™ to the clinical cases where Ultravist™ is contraindicated.

4.5 Utility of the Contrast Agent Evaluation Model

The Contrast Agent Evaluation Model employs SPEKTR generated x-ray spectra, to compute projection data through a cylindrical solid water phantom containing at target contrast agent. Poisson noise added to the projection data allows for computation of CNRp projection data contrast-to-noise ratio computation for the target contrast agent. The image CNR was determined using an empirical correction to account for propagation of noise and other sources of noise. From the computed dose, a "minimum effective concentration" can be determined to compare the performance of contrast agents, for specific kilovoltage and filter combinations.

Very interesting results for the MEC are shown in Table 11 that help provide better understanding of such routine applications as the use of iodine in head applications. As shown, the MEC for iodine at 80 kVp is 0.49 mM while at 120 kVp it is 0.74 mM. This means that for head contrast enhanced CT either 34% smaller amounts of iodine could be used or 57% lower radiation dose could be used by employing 80 kVp rather than 120 kVp! It is surprising that many Radiologists still insist on 120 kVp for such studies!

Table 11 also includes the calculated minimum effective concentration required to produce a contrast-to-noise ratio of one per unit radiation dose (cGy) for iodine at 120 kVp and gadolinium at 120 kVp. As shown the MEC of iodine at 120 kVp 0.74 mM while for gadolinium at 120 kVp it is 0.50 mM. This means for a head contrast enhanced CT either 32% smaller amounts of gadolinium could be used or 54% lower radiation dose could be used by employing gadolinium rather than iodine! These results are clearly in agreement with the phantom results shown in 3.3 and 3.4. The improved performance of gadolinium relative to iodine concurs with the phantom work and animal studies presented.

Finally, an attempt was made to optimize the gadolinium through matching the SPEKTR generated spectrum to the k-edge of gadolinium. This was accomplished by adding a 50 μm W filter to a standard CT system operating at 80 kVp. Figure 28 shows the spectra with the mass attenuation coefficients of gadolinium and iodine superimposed upon it. Since the bulk of the photons in the computed spectra are at or above the k-edge of Gd, excellent contrast is to be expected. The calculated MEC becomes 0.44 mM for Gd at 80 kVp with a 50μm W filter while the MEC for iodine with a standard tube at 120 kVp is 0.74. This means that 41% less contrast would be required or 65% reduced radiation dose is required with this new optimized kV/filter combination and Gd contrast agent.

In a clinical environment, this finding is difficult to verify since such verification would require an invasive change (addition of 50μm tungsten filter) to the system. None-the-less, this finding implies that the use 80 kV with a 50μm tungsten filter could be used to either significantly reduce contrast agent or radiation dose!

Placing additional filters in the path of the x-ray beam will obviously reduce the intensity of the beam. The proposed kVp/filter combination of 80 kVp and 50μm added tungsten results in a reduction of intensity of approximately 84% compared to 120 kVp and no additional filtration added to the permanent 5.0 mm Al. As can be seen from the previous discussion 660 mAs is required compared to 105 mAs at 120 kVp to achieve the same dose to the center of the phantom. Current CT tubes have the capability to provide this mAs with exposure times of 1 second which is a reasonable acquisition time for head CT.

A beam with a narrower energy spectrum would be expected to produce even better contrast enhancement than achieved with the spectrum described (80 kVp with an additional 50*u*m of tungsten). Filtration and appropriate adjustment of kVp that would put the peak of the spectrum just above the k-edge of the contrast material would be ideal for optimizing contrast. This beam, however, would probably be lacking in intensity with the original generator and x-ray tube power. The lack of intensity would limit the utility of such a spectrum until such time as x-ray tubes with sufficient power are developed. A balance of minimizing the spectral width of the spectra used for CT with the desire to have a more monoenergetic beam while maintaining sufficient intensity is one of the possible uses of this model.

The question arises: what would be the effect of increasing the size of the phantom from 16 cm diameter to 32 cm diameter? Would the CT number of the contrast agent change? Would the CNR change? What changes technical factors would need to be made to compensate for these changes?

First, the CT number of a contrast agent might be expected to decrease as the size of the phantom increases. This would be due primarily to hardening of the beam as it passes through the thicker phantom. However, with a well-calibrated CT unit this effect should be small.

Next, if the tube current – time product (mAs) is not changed the noise would be expected to substantially increase due to the increased attenuation of the photons by the larger diameter phantom and subsequent smaller number of photons reaching the detectors. The increase in noise, with a slight decrease in CT number, would dramatically decrease the CNR. Therefore, an increase in the size of the subject will require using higher beam intensity. As expected, this would necessitate one of two changes in the experiment:

1. The MEC would need to increase in order to increase the contrast between the contrast filled vial and the background material, or
2. The mAs would need to increase dramatically in order to decrease the noise of the background material.

The current work has been modeled on a 16 cm diameter water – equivalent phantom which approximates a head. From the above discussion, it can be seen that the next logical step would be to extend this to a body equivalent phantom. This would require calculating a new model, perhaps a 32 cm diameter water – equivalent cylinder. For verification purposes a solid water – equivalent phantom should also be fabricated. Validation of the model to accurately compute CNR_i , dose, and MEC could follow, With validated contrast agent enhancement models available for both head and body, a general Matlab™ application could be readily devised for automatic optimization of "minimum effective concentration" to provide optimum kV's and filtration for any potential contrast agent.

Finally, it appears that an improved version of the Inverse Radon Transform is now available from MathWorks® for MatLab (version R2016a)[84]. It would be interesting for future work, to explore the capabilities of this software for producing useful pseudo images for analysis.

Bibliography

1. Bushberg,2002: Bushberg J, Seibert J A, Leidholdt E, Boone J: The Essential Physics of Medical Imaging; Lippincott Williams & Wilkins, Philadelphia, 2002 page 97
2. Bushberg,2002: Bushberg J, Seibert J A, Leidholdt E, Boone J: The Essential Physics of Medical Imaging; Lippincott Williams & Wilkins, Philadelphia, 2002 page 99
3. Bushberg,2002: Bushberg J, Seibert J A, Leidholdt E, Boone J: The Essential Physics of Medical Imaging; Lippincott Williams & Wilkins, Philadelphia, 2002 page 105
4. C. R. Hammond. *The Elements, in Handbook of Chemistry and Physics 81th edition*. CRC press. ISBN 0849304857
5. Daintith, John. *Facts on File Dictionary of Chemistry, 4th ed.*. New York: Checkmark Books. (2005)
6. Bushong S Radiological Science for Technologists, Mosby Elesvier, St. Louis MO 2008 pages 126-129
7. Bushong S Radiological Science for Technologists, Mosby Elesvier, St. Louis MO 2008 page 122
8. Bushberg,2002: Bushberg J, Seibert J A, Leidholdt E, Boone J: The Essential Physics of Medical Imaging; Lippincott Williams & Wilkins, Philadelphia, 2002 page 100
9. Bushong S Radiological Science for Technologists, Mosby Elesvier, St. Louis MO 2008 page 133
10. 21 CFR 1020: US Code of Federal Regulations Title 20 Section 1020

11. Bushberg,2002: Bushberg J, Seibert J A, Leidholdt E, Boone J: The Essential Physics of Medical Imaging; Lippincott Williams & Wilkins, Philadelphia, 2002 pages 114 -116
12. Carlton R, Adler A: Principles of Radiographic Imaging an Art and a Science, Thompson Delmar Learning, Clifton Park NY 2006 pages 106 and 119
13. Skrukas J: Radiographic Contrast Agents; Aspen Publishers, Rockville MD, 1989 (Skrukas J, editor)
14. Dawson P: Conventional Angiography in Radiographic Contrast Agents; Aspen Publishers, Rockville MD, 1989 (Skrukas J, editor)
15. Sage M: Neuroangiography in Radiographic Contrast Agents; Aspen Publishers, Rockville MD, 1989 (Skrukas J, editor)
16. Bureau of Radiological Health (no authors listed): Radiological Health Handbook, US Dept. of Health, Education, and Welfare Bureau of Radiological Health; Rockville MD, 1970
17. Birch R, Marshall M Adran G M: Catalogue of Spectral Data for Diagnostic X-rays; The Hospital Physics Association; London, 1979
18. Rubin G.D., Duke M.D. and. Napel S.A *et al.*: Three-dimensional Spiral CT angiography of the Abdomen: initial clinical experience, *Radiology* **186** (1993), pp. 147–152.
19. Ricker O., Duber C.and Schmiedt W. *et al.*: Prospective comparison of CT angiography of the legs with intraarterial digital subtraction angiography, *Am J Roentgenol* **166** (1996), pp. 269–276.
20. Tins B., Oxtoby J.and Patel S.: Comparison of CT angiography with conventional arterial angiography in aortoiliac occlusive disease, *Br J Radiol* **74** (2001), pp. 219–225.

21. Alberico R., Patel M.and. Casey S *et al.*: Evaluation of the Circle of Willis with three-dimensional CT angiography in patients with suspected intracranial aneurysms, *Am J Neuroradiol* **16** (1995), pp. 1571–1578.
22. . Gluck B.S and. Mitty H.A: Reactions to iodinated radiographic contrast agents: how to identify and manage patients at risk, *Postgrad Med* **88** (1990), pp. 187–194.
23. Yamagushi K., Katayama H.and Takashima T.*et al.*: Prediction of severe adverse reactions to ionic and nonionic contrast media in Japan: Evaluation of pretesting. A report from the Japanese Committee on the Safety of Contrast Media, *Radiology* **178** (1991), pp. 363–367.
24. Niendorf H.P., Haustein J and Lonton A.T.*et al.*: Safety and tolerance after intravenous administration of 0.3 mmole/kg Gd-DTPA: results of a randomized, controlled trial, *Invest Radiol* **26** (1991) (Suppl 1), pp. 221–223.
25. Thurner SA, Capelastegui A, Herraiz Del Olmo F, et al. Safety and effectiveness of single- versus triple-dose gadodiamide injectionenhanced MR angiography of abdomen: a phase III double-blind multicenter study. Radiology 2001; 219:137–144.
26. Agarwal, R, Brunelli S, Williams K, Mitchell M, Feldmen H, Umscheid C *Gadolinium-based Contrast Agents and Nephrogenic Systemic Fibrosis:A Systematic Review and Meta-analysis* Nephro Dial Transplant 2008.
27. Martin DR, et.al. *Decreased Incidence of NSF in Patients on Dialysis After Changing Gadolinium Contrast-Enhanced MRI Protocols* Journal of Magnetic Resonance Imaging 31:440-446 (2010).

28. Martin DR, Semelka RC, Chapman MD, et.al.: *Nephrogenic Systemic Fibrosis Versus Contrast-Induced Nephropathy: Risks and Benefits of Contrast-Enhanced MR and CT in Renally Impaired Patients*; J. Magn. Reson. Imaging 2009;30:1350-1356
29. Brasch R.C., Introduction to the Gadolinium class, *J Comput Assist Tomogr* **17** (1993) (Suppl 1), pp. S14–S18.
30. Bloem JL, Wondergem J. Gd-DTPA as a contrast agent in CT. Radiology 1989; 171:578–579.
31. Quinn AD, O'Hare NJ, Wallis FJ, et al. Gd-DTPA: an alternative contrast medium for CT. J Comp Assis Tomogr 1994; 18:634–636.
32. Luboldt W, De Santis M, Von Smekal A, et al. Attenuation characteristics and application of gadolinium-DTPA in fast helical computed tomography. Invest Radiol 1997; 32:690–695.
33. Kawano T, Ishijima H, Nakajima T, et al. Gd-DTPA: a possible alternative contrast agent for use in CT during intraarterial administration. J Comput Assist Tomogr 1999; 23:939–940.
34. Gupta AK, Alberico RA, Litwin A, et al. Gadopentetate dimeglumine is potentially an alternative contrast agent for three-dimensional computed tomography angiography with multidetector-row helical scanning. J Comput Assist Tomogr 2002; 26:869–874.
35. Karcaaltincaba M, Foley WD. Gadolinium-enhanced multidetector CT angiography of the thoracoabdominal aorta. J Comput Assist Tomogr 2002; 26:875–878.
36. Budoff MJ, Lu B, Mao S. Gadolinium-enhanced Three-dimensional electron beam coronary angiography. J Comput Assist Tomogr 2002
37. Radon J H: U¨ ber die Bestimmung von Funktionen durch ihre Integralwerte la¨ngs gewisser Mannigfaltigkeiten; *Ber. vor S¨achs. Akad. Wiss.* **69** 262

38. Yang GZ and Firmin D; The Birth of the First CT Scanner; IEEE Engineering in Medicine and Biology 2000 January/February

39. Brooks 1980: Brooks R; "Comparative Evaluation of CT Scanner Technology" in Medical Physics Monograph No. 6 Medical Physics of CT and Ultrasound; Fullerton G D and Zagzebski J A, ed.; American Institute of Physics, NY 1980

40. LeMay 1976: LeMay CEG United States Patent 3,973,128 August 3, 1976

41. Hsieh (2003); Hsieh J:Computed tomography: principles, design, artifacts, and recent advances; Society of Photo-Optical Instrumentation Engineers, Bellingham WA, 2003

42. Kalender W: X-Ray Computed Tomography; Phys. Med. Biol. **51** (2006) R29–R43

43. Moore W, Bonvento M, Olivieri-Fitt R: *Comparison of MDCT Radiation Dose: A Phantom Study* AJR 2006; 187:W498–W502)

44. Wittram C, Meehan MJ, Halpern EF, Shepard JA, McLoud TC, Thrall JH. Trends in thoracic radiology over a decade at a large academic medical center. *J Thorac Imaging* 2004;19 : 164-170

45. Rogers LF. Radiation exposure in CT: why so high? (editorial) *AJR* 2001; 177:277

46. Rogers LF. Serious business: radiation safety and radiation protection. (editorial) *AJR* 2001; 177 : 1

47. Thornton FJ, Paulson EK, Yoshizumi TT, et al. Single versus multi-detector row CT: comparison of radiation doses and dose profiles. *Acad Radiol* 2003;10 : 379-385

48. Hunold P, Vogt F, Schmermund A, et al. Radiation exposure during cardiac CT: effective doses at multi-detector row CT and electron beam CT. *Radiology* 2002;226 : 145-152

49. Hamberg LM, Rhea JT, Hunter GJ, et al. Multi-detector row CT: radiation dose characteristics. *Radiology*2003; 226:762 -772

50. Moro L, Bolsi A, Baldi M, et al. Single-slice and multi-slice computerized tomography: dosimetery comparison with diagnostic reference dose levels [in Italian]. *Radiol Med (Torino)*2001; 102:262 -265
51. Giacomuzzi SM, Torbica P, Rieger M, et al. Radiation exposure in single slice and multi-slice spiral CT (a phantom study). *Rofo* 2001; 173:643 -649
52. Mayo JR, Aldrich J, Müller NL. Radiation exposure at chest CT: a statement of the Fleischner Society. *Radiology*2003; 228:15 -21
53. Shirmpton PC, Jones DG, Hillier MC, et al. *Survey of CT practice in the UK. II. Dosimetric aspects*. NRPB report no R-249. Chilton, England: National Radiological Protection Board,1991
54. Shrimpton PC, Edyvean S. CT scanner dosimetry. *Br J Radiol* 1998; 71:1 -3
55. Lee KS, Primack SL Staples CA, et al. Chronic infiltrative lung disease: comparison of diagnostic accuracies of radiography and low-and conventional-dose thin-section CT. *Radiology*1994; 191:669 -673
56. United Nations Scientific Committee of the Effects of Atomic Radiation. *Source and effects of ionizing radiation: UNSCEAR 1993 report to the General Assembly*, with scientific annexes. New York, NY: United Nations, 1993
57. [No authors listed]. *Documents of the MRPB National Radiological Protection Board. III*. Chilton, England: National Radiological Protection Board, 1992:1 -16

58. Groves AM, Owen KE, Courtney HM, et al. 16-detector multislice CT: dosimetry estimation by TDL measurement compared with Monte Carlo simulation. *Br J Radiol* 2004;77 : 662-665

59. Bonvento M, Moore W, Button T, Weinmann HJ, Yakupov R, Dilmanian FA: *CT Angiography With Gadolinium-Based Contrast Media* Acad Radiol 2006; 13:979–985.

60. J. M. Idée, H. Beaufils, and B. Bonnemain, "Iodinated media-induced nephropathy: pathophysiology, clinical aspects, and prevention", *Fundamental & Clin. Pharmacol.* 8, pp. 193-206, 1994.

61. A. Meyrier, "Nephrotoxicity of iodine contrast media", *Annales de Radiologie* 37, pp. 286-295, 1994.

62. R. Mikkonen, T. Kontkanen, and L. Kivisaari, "Late and acute adverse reactions to iohexol in a pediatric population", *Pediatr. Radiology* 25, pp. 350-352, 1995.

63. E.C. Lasser, S. G. Lyon, and C. C. Berry, "Reports on Contrast Media Reactions: Analysis of Data from Reports to the U.S. Food and Drug Administration", *Radiology* 203, pp. 605-610, 1997.

64. R. W. Katzberg, "Urography into the 21st Century: New Contrast Media, Renal Handling, Imaging Characteristics, and Nephrotoxicity", *Radiology* 204, pp. 297-312, 1997.

65. F. A. Dilmanian, H. J. Weinmann, Z. Zhong, T. Bacarian, et al. "Tailoring X-Ray Beam Energy Spectrum to Enhance Image Quality of New Radiography Contrast Agents Based on Gd or Other Lanthanides" in "Progress in Biomedical Optics and Imaging", Vol. 2, No. 25, L. E. Antonuk and M. J. Yaffe, eds. Proceedings of SPIE Vol. 4320), "Physics of Medical Imaging", pp 417-426, 2001.

66. Kim J L, Kim BH, Chang S Y, Lee J k: Establishment of ANSI N13.11 X-ray Radiation Fields for Personal Dosimetry Performance Test By Computation and Experiment, *Environ Health Perspect 105, Suppl. 6 Dec 1997*.

67. Storm E: Emission of Characteristic L and K Radiation from Thick Tungsten Targets, *J. Appl. Phys., Vol. 43, No. 6, June 1972*.

68. Morin R L, Raeside D E: Bremsstrahlung Spectra Sampling for Monte Carlo Simulations, *Phys. Med. Biol., Vol. 27, No. 2, 223-228, 1982*

69. International Commission on Radiation Units and Measurements (no author given): Stopping Powers for Electrons and Positrons. ICRU Report no 37. Bethesda, MD, 19985

70. Attix F H: Introduction to Radiological Physics and Radiation Dosimetry, Wiley-VCH, Weinham, FRG, 2004, page 572

71. Attix F H: Introduction to Radiological Physics and Radiation Dosimetry, Wiley-VCH, Weinham, FRG, 2004, page 206

72. Boone J M, Seibert J A: An Accurate Method For Computer Generating Tungsten Anode X-Ray Spectra From 30 – 140 kV, *MedPhys, Vol. 24, No. 11, 1661-1670, 1997*

73. Siewerdsen J H, Waese A M, Moseley D J, Jaffray D A: Spektr: A Computational Tool For X-Ray Spectral Analysis and Imaging System Optimization, *Med. Phys. Vol. 31, No. 11, 3057-3067, 2004*

74. General Electric Product Data Sheet Lightspeed 16 Zero Release B7868 JD/JE/JF

75. Tothill P The ratio of K characteristic to total radiation emitted from a tungsten target X-ray tube *J. Phys. D: Appl. Phys.* 1 1093.

76. Nickoloff E L, Berman HL *Factors Affecting X-Ray Spectra* RadloGraphics 1993; 13:1337-1348

77. Rose A, The sensitivity performance of the human eye on an absolute scale, *J Opt Soc Am* **38:** (1948), pp. 196–208.

78. J.W. Hensona, R.G. Nogueiraa and D.J. Covarrubiasa *et al.*, Gadolinium-enhanced CT angiography of the Circle of Willis and neck, *Am J Neuroradiol* **25** (2004), pp. 969–972.

79. P. Jau, J. Bonnet and P. Joly *et al.*, Etude de l'infareus du myocarde recent en imagere par resonance magnetique avec injection de Dota-gadolinium, *Arch Mal Coeur* **84** (1991), pp. 195–200.

80. M. Remy-Jardin, J. Bahepar and J. Lafitte *et al.*, Multi-detector row CT angiography of pulmonary circulation with gadolinium based contrast agents: prospective evaluation in 60 patients, *Radiology* **238** (2006), pp. 1022–1035.

81. D. D. Cody, D. Pfeiffer, M. F. McNitt-Gray, T. G. Ruckdeschel, K. J. Strauss, P. Wilcox: 2012 Computed Tomography Quality Control Manual; American College of Radiology, 2012, pg. 64

82. E. Rabinowicz: An Introduction to Experimentation; Addison-Wesley, 1970, pg. 19 & 44

83. M. L. Boas: Mathematical Methods in the Physical Sciences 3rd Edition; John Wiley & Sons, Inc., 2006, pg. 762

84. MathWorks®: R2016a Documentation; Natick, MA, 2016